

Irreversible adsorption from dilute polymer solutions

B. O'Shaughnessy^{1,a} and D. Vavylonis^{1,2,b}

¹ Department of Chemical Engineering, Columbia University, 500 West 120th Street, New York, NY 10027, USA

² Department of Physics, Columbia University, 538 West 120th Street, New York, NY 10027, USA

Received 13 January 2003 /

Published online: 8 July 2003 – © EDP Sciences / Società Italiana di Fisica / Springer-Verlag 2003

Abstract. We study irreversible polymer adsorption from dilute solutions theoretically. Universal features of the resultant non-equilibrium layers are predicted. Two broad cases are considered, distinguished by the magnitude of the local monomer-surface sticking rate Q : chemisorption (very small Q) and physisorption (large Q). Early stages of layer formation entail single-chain adsorption. While single-chain physisorption times τ_{ads} are typically micro- to milli-seconds, for chemisorbing chains of N units we find experimentally accessible times $\tau_{\text{ads}} = Q^{-1} N^{3/5}$, ranging from seconds to hours. We establish 3 chemisorption universality classes, determined by a critical contact exponent: zipping, accelerated zipping and homogeneous collapse. For dilute solutions, the mechanism is accelerated zipping: zipping propagates outwards from the first attachment, accelerated by occasional formation of large loops which nucleate further zipping. This leads to a transient distribution $\omega(s) \sim s^{-7/5}$ of loop lengths s up to a maximum size $s^{\max} \approx (Qt)^{5/3}$ after time t . By times of order τ_{ads} the entire chain is adsorbed. The outcome of the single-chain adsorption episode is a monolayer of fully collapsed chains. Having only a few vacant sites to adsorb onto, late-arriving chains form a diffuse outer layer. In a simple picture we find for both chemisorption and physisorption a final loop distribution $\Omega(s) \sim s^{-11/5}$ and density profile $c(z) \sim z^{-4/3}$ whose forms are the same as for equilibrium layers. In contrast to equilibrium layers, however, the statistical properties of a given chain depend on its adsorption time; the outer layer contains many classes of chain, each characterized by a different fraction of adsorbed monomers f . Consistent with strong physisorption experiments, we find the f values follow a distribution $P(f) \sim f^{-4/5}$.

PACS. 82.35.-x Polymers: properties; reactions; polymerization – 05.40.-a Fluctuation phenomena, random processes, noise, and Brownian motion – 68.08.-p Liquid-solid interfaces

1 Introduction

Polymer layer formation is unavoidable when even weakly attractive surfaces come into contact with a polymer solution [1, 2], see Figure 1. Even for extremely dilute polymer solutions, polymer layers develop with densities which may be many orders of magnitude larger than the bulk polymer concentration [3]. This is due to the fact that by giving up their bulk translational entropy, which costs a free energy of only kT , chains achieve an energy advantage proportional to the number of monomers per chain, N , for large enough N values. The topologically complex interfacial layers contain both surface-bound segments and large loops and tails extending into the bulk (see Fig. 1). In principle, given enough time, adsorbed polymers are able to explore all accessible states [4–6] and the layer attains equilibrium. Equilibrium layers have been the focus of a large body of experimental [2, 7–9], theoretical [1–3, 10–20] and numerical [21–23] work.

In a great many cases, however, the surface sticking energy per monomer ϵ exceeds $k_B T$. Available experimental evidence suggests that desorption processes and relaxation kinetics within the layer are then sharply slowed down [24–40]. For ϵ values of several $k_B T$ time scales become so long that the layer build-up becomes essentially an irreversible process leading to non-equilibrium structure [31, 32]. One may speculate this is due to cooperative effects mediated by mutual topological chain constraints which drastically suppress mobilities near the surface [40]. Indeed, in the scaling theory [1] for equilibrium layers, when ϵ exceeds $k_B T$ the smallest loops in the layer become as small as the monomer size, a . Such small loops are likely to greatly restrict chain motion.

For physical-adsorption processes, large sticking energies originate in hydrogen bonding, dispersion or dipolar forces or attractions between charged groups. Most metal and silicon-based surfaces are normally oxidized and many polymer species form strong hydrogen bonds with the surface oxygen or silanol groups. Biopolymers such as proteins and DNA attach tenaciously to many surfaces due

^a e-mail: bo8@columbia.edu

^b e-mail: dv35@columbia.edu

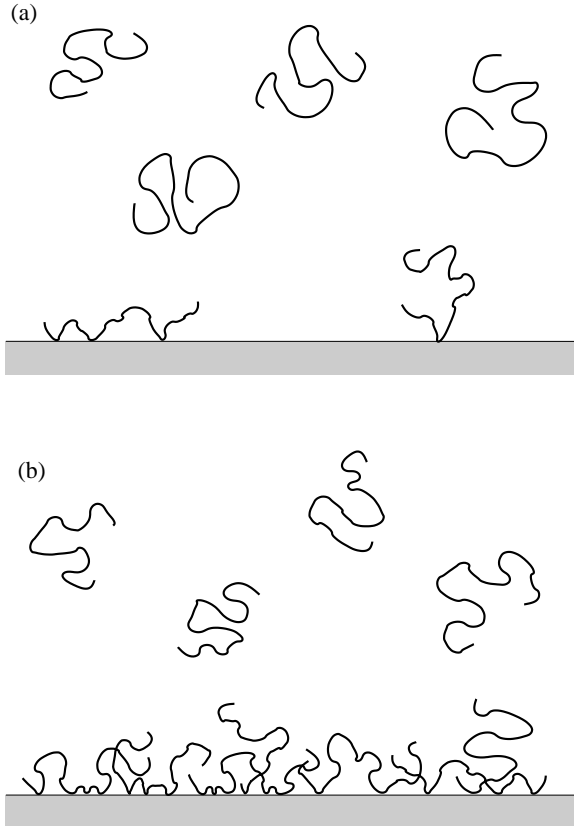


Fig. 1. The situation studied in this paper: polymer chains adsorbing onto a surface from a dilute polymer solution. We consider situations where monomer-surface bonds develop irreversibly, due either to chemical bonding or strong physical interactions. (a) Early stages of layer formation. The surface is almost empty and the first chains to arrive adsorb on the surface without interference from others. (b) At longer times a polymer layer of strongly interacting chains develops and chain densities on the surface become much higher than those in the bulk.

to their large number of charged and polar groups [41, 42]. Since hydrogen bonds, for instance, normally have energies of $4k_B T$ and greater [43], it is apparent that strong physical bonds are very common.

The extreme example of irreversibility arises in *chemisorption* [44–48] where covalent surface-polymer bonds develop irreversibly (Fig. 1). In various technologies polymers are attached by chemical reactions to solid surfaces either from solution as in colloid stabilization by chemically grafting polymers onto particle surfaces [49], or from a polymer melt as occurs in the reinforcement of polymer-polymer [50–52] or polymer-solid [50, 53–55] interfaces. In general, whether physical or chemical bonding is involved, many applications prefer the strongest and most enduring interfaces possible and irreversible effects are probably the rule rather than the exception.

This paper considers dilute solutions. Irreversible adsorption from melts and semidilute solutions, previously studied both experimentally [56–63] and theoretically [64–66], involves rather different processes. Our aim is to understand the structure and formation kinetics of layers

which are formed under these irreversible circumstances where the usual statistical mechanical approach is inapplicable to the non-equilibrium structures which form. A series of experiments by Granick and coworkers [27–35] have examined these issues. These workers found that when ϵ reached values of only a few $k_B T$, polymer relaxation times became large and equilibrium layers were not attained. This was most clearly apparent in experiments following polymethylmethacrylate (PMMA) adsorption onto oxidized silicon ($\epsilon \approx 4k_B T$) via hydrogen bonding from a dilute CCl_4 solution [30–33]. Measuring both the total adsorbed mass, Γ , and the surface-bound part, Γ_{bound} , as a function of time by infrared absorption spectra, it was found that early-arriving chains had much higher fractions of bound monomers, f , than late arrivers, and these f values were frozen in throughout the experiment's duration of several hours. Essentially, monomers remained irreversibly fixed to the site they originally landed on, or at least close to this site. Measuring the distribution of f values among chains they found a bimodal distribution shown in Figure 2(b) with two peaks at small and large f , respectively. This is strikingly different to equilibrium layers where all chains within the layer are statistically identical and are characterized by the *same* time-averaged value, $f = \Gamma_{\text{bound}}^{\infty}/\Gamma^{\infty}$, where ∞ denotes asymptotic values ($t \rightarrow \infty$).

A number of analytical and numerical efforts [32, 46, 47, 67–71] have addressed irreversible polymer adsorption from solution. However, the understanding of these phenomena remains very far from the quantitative level which has been achieved for equilibrium layers. In this paper we develop a theory which amongst other objectives aims to understand the experimental findings of references [30–33]. We emphasize adsorption from a dilute polymer solution under good-solvent conditions and consider systems where monomer-surface bonds are strong enough that they are effectively irreversible within the experimental timescales. Certain results are generalized to theta-solvent solutions. We calculate the relationship $\Gamma_{\text{bound}}(\Gamma)$, how each of Γ_{bound} and Γ depends on time, as well as the final layer's distribution of chain contact fractions, $P(f)$. We will compare our predicted final layer structure to the well-established theoretical results for equilibrium layers which predict a density profile $c(z) \sim z^{-4/3}$, and a self-similar loop distribution, $\Omega(s) \sim s^{-11/5}$. Similar to the picture that was developed by Granick and coworkers, we find that the final layer consists of two populations: early-arriving chains lie flat on the surface while late arrivers can only adsorb with an ever-decreasing fraction of their monomers onto the surface leading to a diffuse weakly attached outer layer. We find a universal distribution of f values, $P(f) \sim f^{-4/5}$ for small f which agrees rather closely with the experiments of references [31, 32]. Interestingly, we find layer loop distributions and density profiles obeying the same scaling laws as those of equilibrium layers. Chain configurations are very different, however, leading to radically different physical properties of the layer.

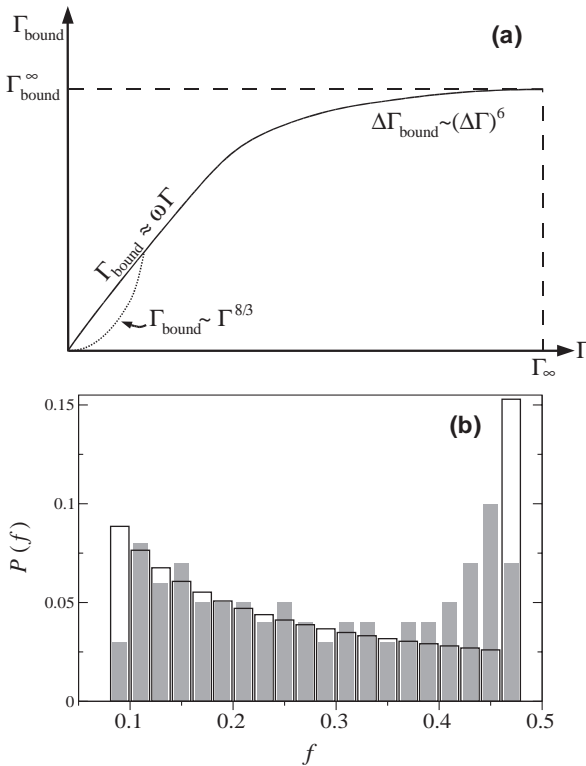


Fig. 2. (a) Theoretically predicted dependence of surface-bound mass, Γ_{bound} , on total adsorbed mass per unit area, Γ . For irreversible physisorption, an initial linear regime crosses over to sharp saturation $\Delta\Gamma_{\text{bound}} \sim (\Delta\Gamma)^6$ as asymptotic coverages are approached. A similar curve has been measured experimentally in reference [31]. For chemisorption the relation is the same, but with an additional initial regime $\Gamma_{\text{bound}} \sim \Gamma^{8/3}$. (b) Probability distribution of fraction of bound monomers f per chain. Grey bars reproduce experimental data from reference [31]. Empty bars are the theoretically predicted $P(f) \sim f^{-4/5}$ for $f_{\min} < f < \omega$, where values for $f_{\min} = 0.09$ and $\omega = 0.47$ were derived from the measurements in reference [31]. The delta-function at $f = \omega$ is the contribution from early-arriving chains and is expected to be broadened in reality.

Our picture of irreversible polymer adsorption is in some respects qualitatively similar to the theoretical one of the workers of reference [32] who simulated their experiments in a random sequential adsorption [72] framework. They visualized chains as “deformable droplets”: at the early stages when the coils arrive onto a bare surface, each droplet adsorbs a certain maximum cross-sectional area. As available surface area for adsorption become scarce, in order for late-arriving chains to adsorb, it was assumed droplets deform by reducing their cross-sectional areas parallel to the surface to fitting into the empty space. In so doing, they become more extended into the bulk. Using this model they generated a $P(f)$ similar to the experimental one of Figure 2(b). The picture developed here differs in this respect: late-arriving chains freely overhang early flat-lying chains and rather than fitting into a single available connected surface area, they attach at disconnected empty surface sites.

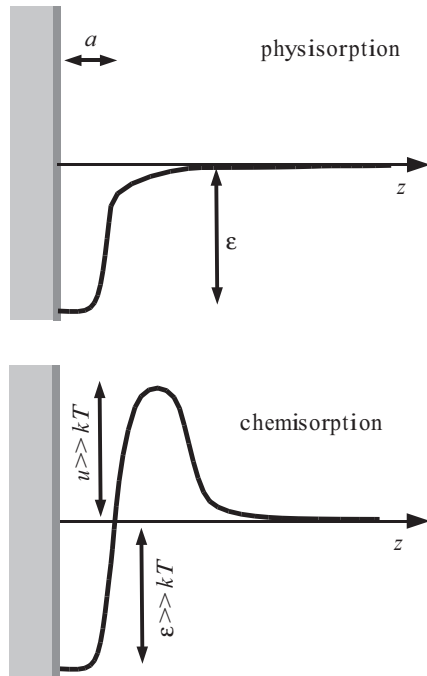


Fig. 3. The two classes studied in this paper: physisorption and chemisorption. Simplified view of monomer free energy as a function of distance between monomer and surface. In physisorption there is no activation barrier and monomer-surface association is immediate upon contact. When sticking energy ϵ exceeds a few kT , experiment indicates that effective desorption rates become very small, presumably due to complex many-chain effects. Chemisorption typically involves a large activation barrier, $u \gg kT$, which needs many monomer-surface collisions to traverse. The adsorption strength is also large, $\epsilon \gg kT$. Some systems are in practice mixtures of chemi and physisorption, a complexity not dealt with in the present work.

The process of irreversible polymer layer formation entails progressive freezing-in of constraints due to irreversible monomer-surface bonding. These constraints gradually reduce the volume of configurational phase space available. Thus, ergodicity is inapplicable and in lieu of the algorithms of equilibrium statistical mechanics, one must follow the kinetics of chain adsorption and layer build-up. It is important to distinguish carefully between two broad classes of adsorption kinetics, physisorption and chemisorption, which are characterized by very different values of the local reaction rate Q . We define this as the conditional monomer-surface reaction rate, given an unattached monomer contacts the surface (see Fig. 3). In physisorption, monomer attachment is essentially diffusion-limited, $Q \approx 1/t_a$, where t_a is the monomer relaxation time. Chemisorption, where adsorbed monomers form very strong chemical bonds with the surface [44–48, 73] is much slower [52, 74, 75] with Q values 8 or more orders of magnitude smaller than those of physisorption. The origin of this difference is that chemical bond formation usually involves a large activation barrier (Fig. 3).

Our theoretical approach is to make the simple assumption of total irreversibility, motivated by the experiment discussed above: once a monomer bonds with the surface, our model is that this bond never breaks. The processes of chemisorption and physisorption will be analyzed separately. Though we find both lead to similar final layer structures, the kinetics are very different. In physisorption, a single chain adsorbs onto a bare surface in a time of order the coil relaxation time or less, typically microseconds, whereas single-chain chemisorption may last minutes or even hours and is thus observable experimentally. We begin with a study of chemisorption in Sections 2, 3, and 4. Specifically, in Section 2 we show that quite generally there are three possible modes of single-chain adsorption, depending on the value of a certain critical exponent θ . Single-chain chemisorption from good and theta solvents is then studied in detail in Section 3. In Section 4 we consider the later stages of the kinetics when chains overlap and dense layers are formed (Fig. 1). The case of irreversible physisorption is treated in Section 5. We compare our results to experiment and conclude with a discussion in Section 6. An announcement of our results has appeared in reference [76].

2 Chemisorption, general discussion: three modes of adsorption

Our interest is an initially bare surface confronting a dilute solution of functionalized chains. During the earlier stages of surface layer formation, the coverage is small and individual chains do not see each other. In this section, we consider in detail how a single chain chemisorbs onto an interface, remembering that chemisorption is characterized by very small values of the local monomer-surface reaction rate Q . The chain will make an initial attachment and then develop a certain loop profile as successive monomers gradually attach, eventually leading to complete chain adsorption in a certain time τ_{ads} (see Fig. 4), whose dependence on chain length is an important characteristic. Since the early polymer layer consists of chains dilute on the surface as in Figure 1(a), the initial layer structure is a superposition of these single-chain loop profiles.

In this section we consider chemisorption in its full generality. We show that there are three distinct classes of behavior, each with different adsorption modes, loop profiles and adsorption times τ_{ads} . Which class a given experimental system belongs to depends on the bulk concentration regime and other factors. The classes are defined by the value of a critical exponent characterizing polymer statistics near surfaces.

We will assume that all monomers are identical and chemically active, and that the surface has a free energetic preference for the solvent over the polymer species. This means that in terms of physical interactions the polymers see a hard, repulsive wall. We choose units where the monomer size a is unity.

Consider the chain in Figure 4(b) whose first monomer has just reacted with the surface. Which of the chain's remaining monomers will react next? What is the sequence

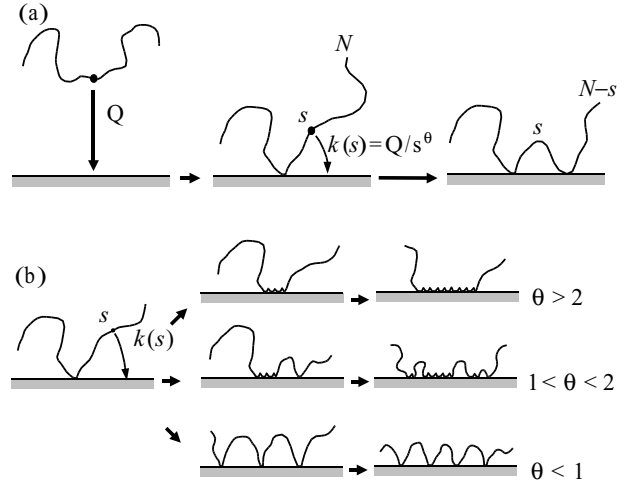


Fig. 4. Schematic of single-chain chemisorption. (a) A chain makes its first attachment with the surface and starts its adsorption process. The rate of first monomer attachment is proportional to Q , namely the reaction rate given the monomer touches the surface. Subsequent monomer adsorption is determined by the form of the reaction rate $k(s)$ for the s -th monomer away from the first attachment. For $s \ll N$, where N is the length of the tail, $k \approx Q/s^\theta$ where the exponent θ reflects equilibrium polymer statistics near interfaces, given the constraints imposed by earlier reactions. (b) Depending on θ , three modes of adsorption are possible. i) Zipping, $\theta > 2$. Monomers adsorb sequentially forming a long train. ii) Accelerated zipping, $1 < \theta < 2$. As i) but zipping is accelerated by nucleation of new zipping centers due to formation of large loops. iii) Uniform collapse ($\theta < 1$). Monomers distant from adsorbed ones come down first leading to formation of large loops whose size is uniformly decreasing with time. Chemisorption from dilute solution with good solvent is accelerated zipping ($\theta = 8/5$).

of chemisorption events? This depends on the form of the reaction rate $k(s)$ at which a reactive group s monomer units along the backbone away from the bound monomer reacts with the surface, as shown in Figure 4(a). Now the important feature of chemisorption is that due to the smallness of Q in order for any chemical bond to form a time much larger than the attached chain's relaxation time is needed. Thus, quite generally the reaction rate for a given monomer at any moment is proportional to the equilibrium contact probability of finding this monomer on the surface given the current constraints due to all chemical bonds formed at earlier times. In this particular situation, this is

$$p(s|N) = \frac{Z(s, N)}{Z(N)}, \quad (1)$$

where $Z(N)$ is the partition function of the chain with one monomer bound (middle of Fig. 4(a)) and $Z(s, N)$ is the partition function of the chain which has the additional constraint that the s -th monomer is also bound (last of Fig. 4(a)). Physically, one expects that for small enough s , this is independent of N , *i.e.* $p(s|N) \approx s^{-\theta}$, where the value of the exponent θ reflects the equilibrium polymer

statistics, given the constraints. This then leads to the following expression for the reaction rate:

$$k(s) \approx \frac{Q}{s^\theta} \quad (s \ll N). \quad (2)$$

The total reaction rate for the next adsorption event is a sum over all the $N - 1$ monomers which may adsorb next. These belong to the two tails in Figure 4(b) which are of order N in length. The net reaction rate is thus approximately

$$\mathcal{R}_{\text{total}} \approx \int_1^N k(s) ds, \quad (3)$$

which, depending on the value of θ , is dominated by either small or large s .

This argument is then repeated for the reactions of the second, third and subsequent monomers, in all cases described by a rate with the same small- s behavior as in equation (2). The only difference is that tails are replaced by loops. Thus, the entire kinetic sequence is characterized by the single exponent θ . The nature of the kinetics depends on the value of θ as follows.

- i) $\theta > 2$. Suppose the equilibrium statistics (Eq. (1)) are such that $k(s)$ decays faster than $1/s^2$. Then $\mathcal{R}_{\text{total}} \approx k(1)$ and typically a monomer near the first attachment is most likely to attach next. The third monomer to attach, repeating the same argument, will be near the first two, and so on. In this case, therefore, the chain would *zip* onto the surface starting at the first attachment point, as shown in the top of Figure 4(b). Since each new attachment occurs at the same rate each time, the full zipping time would then be $\tau_{\text{ads}} \approx N/k(1) \approx Q^{-1}N$.
- ii) $\theta < 1$. In this case $\mathcal{R}_{\text{total}}$ is dominated by s of order N reflecting the fact that even though a monomer with small s is, on average, more frequently near the surface than a distant one, there are many more distant ones and their number is the dominating factor. Thus, a distant monomer of order N units away from the first graft attaches next, leading to the formation of a loop of size of order N . Repeating the argument for the subsequent reactions leads to a process of uniform *collapse* of the chain, where roughly centrally positioned monomers of loops react with the surface at each step, as shown in the bottom case of Figure 4(b). In this case, the average lifetime of a loop with s monomers is $\tau_{\text{loop}}(s) \approx 1/\int_1^s ds' k(s') \approx Q^{-1}s^{1-\theta}$. Thus, smaller loops take longer time to collapse and the rate limiting step for full adsorption is the collapse of the smallest loops: $\tau_{\text{ads}} \approx \tau_{\text{loop}}(1) \approx Q^{-1}$.
- iii) $1 < \theta < 2$. This is intermediate between zipping and collapse. Though $\mathcal{R}_{\text{total}}$ is dominated by small s , suggesting zipping, there is in fact enough time before pure zipping completes for large loops to form. To see this, return to the 1-graft situation on the extreme left of Figure 4(b). The time for a loop of order N (for the argument's sake, bigger than $N/2$) to form from one

of the two tails extending from the grafted monomer is roughly

$$\tau_N \approx \left(\int_{N/2}^N ds k(s) \right)^{-1} \approx Q^{-1}N^{\theta-1}. \quad (4)$$

This is much smaller than $\tau_{\text{ads}} \sim N$ which pure zipping would give, and thus before pure zipping is complete, large loops must have formed. We call this case *accelerated zipping*, since large loop formation effectively short-circuits the pure-zipping process by nucleating new sources of zipping as shown in the middle case of Figure 4(b). Now equation (4) implies (unlike $\theta < 1$) larger loops take longer to form. Thus by τ_N loops of all sizes have come down, *i.e.* the chain has adsorbed and we conclude $\tau_{\text{ads}} \approx \tau_N$.

In summary, depending on the value of θ the chemisorption time has three possible forms:

$$Q\tau_{\text{ads}} \approx \begin{cases} \text{const} & (\theta < 1), \\ N^{\theta-1} & (1 < \theta < 2), \\ N & (\theta > 2). \end{cases} \quad (5)$$

In the next section we calculate the value of θ under good-solvent conditions and find that it belongs to the accelerated-zipping case. We then study the corresponding case in detail.

3 Single-chain chemisorption in a good solvent: accelerated zipping

In this section we consider the kinetics of single-chain chemisorption, describing polymer layers during the early stages of the chemisorption process, Figure 1(a). Expressions are derived for the number of bound monomers, $\gamma_{\text{bound}}(\tau)$, and the single-chain loop distribution profile, $\omega_\tau(s)$, where τ measures time after first monomer attachment onto the surface. In order to perform these calculations, in this section we first evaluate the reaction exponent θ of equations (2) and (5) and find it belongs to the accelerated-zipping class. Subsequently, we solve the accelerated-zipping kinetics, first using simple scaling arguments and then a more detailed solution of the rate equations.

3.1 The reaction exponent θ

To our knowledge, θ in good solvents has not been calculated before. We show here that it can be expressed in terms of other known critical exponents characterizing polymer networks [77, 78]. The simplest way to derive θ is to consider a loop of N monomers bound to the surface by its two ends as in Figure 5(a). Then the reaction rate of its s -th monomer resulting in the formation of two loops of lengths s and $N - s$, as shown in Figure 5(b), is

$$k(s|N) = Q \frac{Z_{\text{loop}}(s, N - s)}{Z_{\text{loop}}(N)}, \quad (6)$$

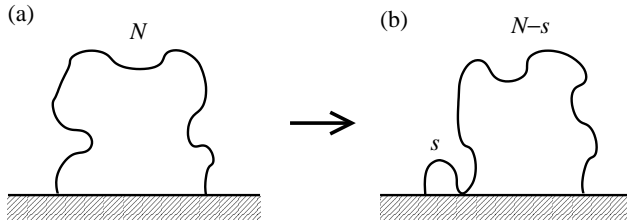


Fig. 5. A polymer loop anchored to the surface by its two ends. The reaction rate of its s -th monomer with the surface, leading to two loops of length s and $N - s$, is proportional to the ratio of the partition functions of the loop before and after the reaction.

where $Z_{\text{loop}}(N)$ and $Z_{\text{loop}}(s, N - s)$ are the partition functions of the loops of Figure 5(a) and (b), respectively. Now although $Z_{\text{loop}}(N)$ is known, $Z_{\text{loop}}(s, N - s)$ is only known for s of order N . From reference [77]:

$$Z_{\text{loop}}(N) \approx \mu^N N^{\gamma_a - 1}, \quad Z_{\text{loop}}(N/2, N/2) \approx \mu^N N^{\gamma_c - 1}, \quad (7)$$

where μ is a constant of order unity and the values of γ_a, γ_c have been calculated analytically and numerically [77, 78]. Now, demanding that $Z_{\text{loop}}(s, N - s)$ follows a power law for small s and that it reduces to equations (7) in the $s \rightarrow 1$ and $s \rightarrow N/2$ limits one has

$$Z_{\text{loop}}(s, N - s) \approx \mu^N N^{\gamma_c - 1} \zeta\left(\frac{s}{N}\right). \quad (8)$$

Here the scaling function ζ must obey:

$$\zeta(x) \approx \begin{cases} x^{-\theta} & (x \rightarrow 0), \\ 1 & (x = 1/2), \\ (1-x)^{-\theta} & (x \rightarrow 1), \end{cases} \quad (9)$$

where the $x \rightarrow 0$ and $x \rightarrow 1$ behaviors are identical by symmetry and

$$\theta = 1 + \nu \approx 8/5 \quad (\text{good solvent}), \quad (10)$$

which follows after using the identity [77] $\gamma_a - \gamma_c = \nu + 1$. Here $\nu \approx 3/5$ is the Flory exponent [79]. From equations (6), (7), and (8) one thus has

$$k(s|N) \approx \frac{Q}{N^\theta} \zeta\left(\frac{s}{N}\right), \quad (11)$$

which for $s \ll N$, reduces to equation (2), $k \sim s^{-\theta}$. Thus, single-chain chemisorption in a good solvent is characterized by $\theta \approx 8/5$; since $1 < \theta < 2$, the adsorption mode is accelerated zipping.

Equation (11) was derived for the particular case of a loop as in Figure 5. But even if the reacting monomer is part of a tail as in Figure 4(a), by a straightforward generalization of the reasoning of this section using the exponents calculated in reference [77], one can show that the reaction rate has the same form for $s \ll N$. One can show the same is true if the ends of the loop in Figure 5 are connected to other loops.

The above results for θ directly generalize to theta-solvent solutions. In this case polymer statistics are effectively ideal [79] and $\nu \rightarrow 1/2$ in all of the above, *i.e.*

$$\theta = 3/2 \quad (\text{theta solvent}), \quad (12)$$

which also corresponds to accelerated zipping. In fact, for this case the exponent can be obtained more simply as follows: the probability that the s -th monomer, measured from a given surface attachment, is in contact with a hard wall is proportional to the return probability P of a random walk which starts one step away from an absorbing surface after s steps, *i.e.* $k \sim P \sim s^{-3/2}$.

Finally, we remark that the partition functions of equation (7) correspond to loops such as those of Figure 5 whose end locations on the surface are annealed [77]. However, for chemisorption onto solid surfaces the ends are either completely fixed or may diffuse very slowly on the surface. (Note that chemisorption onto liquid interfaces are cases where the end locations are truly annealed.) Nonetheless, all our results for $s \ll N$ and the scaling structure of equation (11) must remain the same even in this case, since in the $s \ll N$ limit, $k(s|N)$ is independent of the location of the other end. Our general conclusions are thus expected to be robust, provided the two ends are not so far apart that there are strong lateral loop stretching effects. In the following we self-consistently assume that as the adsorption process proceeds there is no tendency for generated loops to be in such stretched configurations.

3.2 Accelerated zipping: scaling analysis

Let us consider now the kinetics of adsorption starting from a polymer chain as in Figure 4(a) which has just made its first attachment with the surface with an interior monomer. This is in fact typical: we show in Appendix A that chains are much more likely (by a factor $N^{0.48}$) to make their first surface contact with an interior monomer because there are many more (of order N) such monomers as compared to chain ends.

Now the chain starts to chemisorb at $\tau = 0$. From the previous section we have seen that in the accelerated-zipping mode the chain adsorption time τ_{ads} is equal to τ_N , the timescale associated with loops of size N . What will the chain's loop profile be for times τ smaller than τ_N ? Initially, since the reaction rate is dominated by small s , the chain will start to zip and sequences of bound monomers ("trains") will grow outwards from the first attachment point. As time proceeds though, large loops start to come down due to adsorption of monomers distant to the already bound ones. These loops have a certain distribution of loop sizes $\omega_\tau(s)$ and their effect is to accelerate the zipping process since they nucleate further sources of zipping and train formation. The maximum size of such loops which had enough time to form by time τ , *i.e.* for which $\int_{s_\tau^{\max}}^N ds' k(s') \approx 1/\tau$, is

$$s_\tau^{\max} \approx (Q \tau)^{1/\nu}, \quad (13)$$

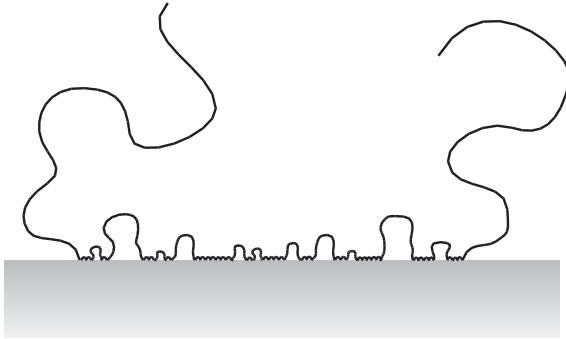


Fig. 6. Snapshot of loop profile of a chemisorbing chain during its accelerated zipping down onto a surface. At an earlier time the chain adsorbed with an interior monomer from which zipping started to propagate outwards accompanied by occasional formation of large loops which nucleated further zipping sources as shown. The distribution of loop sizes follows a universal power law and as larger loops form with increasing time, loop sizes are larger near the outermost tails. The tails act as a continuous loop source, thus sustaining the loop distribution. Eventually, after $\tau_{\text{ads}} \approx Q^{-1} N^\nu$, the largest loop becomes of order the tail size, N , the tails are completely consumed and the structure collapses onto a completely flat configuration.

which increases with time. The maximum loop size thus becomes of order N at τ_N .

Overall, we expect the chain to consist of three parts, shown in Figure 6: i) Two large tails, each of length of order N . These are the two tails of the polymer chain which was initially bound by one of its interior monomers as in Figure 4(a). For $t \ll \tau_N$ the tails had neither enough time to decay into large loops, nor to completely zip. ii) Loops with a loop distribution $\omega_\tau(s)$. iii) Trains of bound monomers whose number we define to be $\gamma_{\text{bound}}(\tau)$.

Now $\gamma_{\text{bound}}(\tau)$ is easily found by making the ansatz that it follows a power law in time. In addition, for short times γ_{bound} is independent of N ; one can imagine sending the chain size to infinity, which would not affect the accelerated zipping propagating outwards from the initial graft point. This dictates

$$\gamma_{\text{bound}}(\tau) \approx N \left(\frac{\tau}{\tau_N} \right)^{1/\nu} \quad (\tau \ll \tau_N), \quad (14)$$

since by τ_N most of the chain has adsorbed, *i.e.* we must have $\gamma_{\text{bound}}(\tau_N) \approx N$.

We now evaluate $\omega_\tau(s)$ by making the ansatz that it also has power law behavior:

$$\omega_\tau(s) \approx \frac{1}{s_\tau^{\max}} \left(\frac{s_\tau^{\max}}{s} \right)^\delta \quad (1 \ll s \ll s_\tau^{\max}), \quad (15)$$

with $\delta > 1$. Since by τ there has been enough time for the formation of order one loop of length s_τ^{\max} , the normalization has been chosen such that there is one loop of order s_τ^{\max} in size. Now the total number of loops is thus $L(\tau) = \int_1^N ds \omega_\tau(s) \approx (s_\tau^{\max})^{\delta-1}$. These loops provide $L(\tau)$ new nucleation points for further zipping. The

reaction rate at each such point is dominated by small s (since $\theta > 1$) and is thus of order $k(1)$, so

$$\frac{d\gamma_{\text{bound}}}{d\tau} \approx k(1)L(\tau) \sim \tau^{(\delta-1)/\nu} \quad (\tau \ll \tau_N). \quad (16)$$

Now demanding that (16) reproduces equation (14) the value of δ is determined:

$$\delta = 2 - \nu. \quad (17)$$

Notice that the above results are self-consistent: the number of loops $L(\tau)$ is much smaller than $\gamma_{\text{bound}}(\tau)$, and essentially all reacted monomers do belong to trains as assumed in equation (14).

Let us summarize this section's results, setting $\nu = 3/5$ which is the value relevant to our main interest of dilute solutions with good solvent. From equations (13), (14) and (15) we have

$$\gamma_{\text{bound}}(\tau) \approx (Q\tau)^{5/3}, \quad \omega_\tau(s) \approx (Q\tau)^{2/3}s^{-7/5} \quad (18)$$

valid for $\tau < \tau_N$ and $s < s_\tau^{\max} \approx (Q\tau)^{5/3}$.

3.3 Accelerated zipping: solution of rate equations

In this section we analyze the accelerated-zipping phenomenon in a more rigorous way by solving the loop evolution dynamics. We will recover all of the scaling results of Section 3.2. The time evolution of the chain's loop distribution is given by [46]

$$\frac{d\omega_\tau(s)}{d\tau} = 2 \int_s^N ds' \omega_\tau(s') k(s|s') - \int_0^s ds' \omega_\tau(s) k(s'|s), \quad (19)$$

where the first term on the right-hand side (rhs) describes the rate of formation of loops of length s by bigger ones, while the second term on the rhs is the rate of decay of a loop of length s into smaller loops [80] and k is given by equation (11). The initial condition for equation (19) is $\omega_0(s) = \delta(s - N)$, *i.e.* there is only one initial loop of length N (in the following, for simplicity, we do not distinguish between tails and loops). A basic assumption in equation (19) is that $k(s|N)$ retains the form of equation (11) throughout the adsorption process. That is, we assume topological and many-loop excluded-volume effects (beyond those contained in Eq. (6)) are not strong enough to alter the essential form of $k(s|N)$. It is easy to show by integrating equation (19) over all s (see calculation in App. B) that the kinetics conserve the total number of monomers. Formally, $\omega_\tau(s)$ in equation (19) is an ensemble average over many chains. However, the number of loops formed by a single chain becomes much larger than unity as time increases and thus equation (19) accurately describes the loop distribution of a single chain as well.

Although both integrals in equation (19) diverge at $s' = s$ and $s' = 0$, these divergences cancel with one another. In fact defining $D_\tau(s)$ to be the number of loops larger than s ,

$$D_\tau(s) \equiv \int_s^\infty ds' \omega_\tau(s'), \quad (20)$$

we obtain the following equivalent rate equation which has well-defined integrals:

$$\frac{dD_\tau(s)}{d\tau} = \int_s^N ds' \lambda(s|s') \omega_\tau(s'), \quad (21)$$

where

$$\begin{aligned} \lambda(s|s') &\equiv \frac{Q}{s'^\nu} \int_{s/s'}^{1-s/s'} dx \zeta(x) \\ &= \begin{cases} -AQ/(s'-s)^\nu & (s' \rightarrow s), \\ BQ/s^\nu & (s' \gg s), \end{cases} \end{aligned} \quad (22)$$

with A, B positive constants of order unity. Equation (21) is derived by integration of equation (19). Its validity is easy to check by differentiation with respect to s and using $\zeta(s/s') = \zeta(1-s/s')$; one then recovers equation (19). Notice that the function $\lambda(s|s')$, which describes how much each loop s' contributes to changes in $D_\tau(s)$, is negative for $s' < 2s$ since a loop shorter than $2s$ always creates at least one loop smaller than s . Also $\lambda(s|s')$ is positive for $s' > 2s$, since at least one loop bigger than s is created by a loop longer than $2s$.

We saw in Section 3.2 that the two large tails forming after the first attachment have of order N monomers until essentially the end of the chemisorption process. In order to describe the tail kinetics, let us consider s very close to N in equation (21):

$$\frac{dD_\tau(s)}{d\tau} \approx - \int_s^N ds' \frac{AQ}{(s'-s)^\nu} \omega_\tau(s') \quad (s \rightarrow N). \quad (23)$$

Self-consistently, one can show that error terms arising from approximating λ by $-AQ/(s'-s)^\nu$ in equation (23) are higher order. Equation (23) is solved in Appendix C, with solution

$$\omega_\tau(s) = \frac{1}{s_\tau^{\max}} \left(\frac{s_\tau^{\max}}{N-s} \right)^{1+\nu} h \left(\frac{s_\tau^{\max}}{N-s} \right) \quad (N-s \ll N),$$

$$\text{where } h(x) \rightarrow \begin{cases} 0 & (x \gg 1), \\ \text{const} & (x \ll 1). \end{cases} \quad (24)$$

The cutoff function $h(x)$ decays to zero exponentially rapidly as $x \rightarrow \infty$. Equation (24) (see Fig. 7) describes the length of the two initial tails, which is continuously decreasing. After time τ , the length has decreased by s_τ^{\max} . This decrease is the maximum loop size that any tail could have created by time τ . Due to fluctuations, the initial δ -function peak broadens as it moves towards $s = 0$. Thus, $\omega_\tau(s)$ in equation (24) is the probability distribution of the tail length. One sees that by time τ_N the length of the tail (the largest non-adsorbed chain segment) shrinks to zero, thus marking the end of the single-chain adsorption process.

Consider now loops ($1 \ll s \ll N$) generated by occasional grafting of distant monomers. For short enough times the only sources of loop formation are the tails which dominate the integral on the rhs of equation (21) at s' of

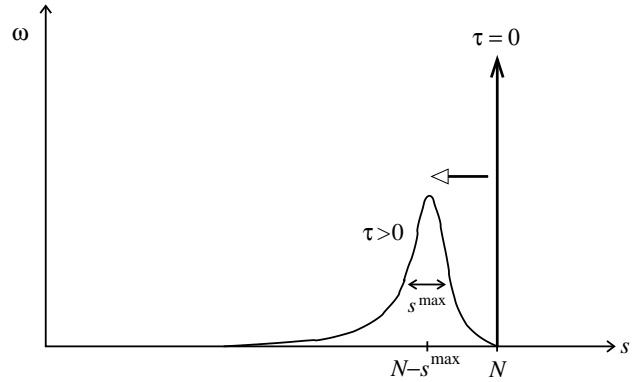


Fig. 7. Sketch of the size probability distribution $\omega_\tau(s)$ for the large tail ($s \rightarrow N$, Fig. 6) for a polymer chemisorbing from a good solvent, see equation (24). The initial ($\tau = 0$) tail length is a δ -function peaked at N and decreases with time τ on average by s_τ^{\max} . The broad distribution at τ represents fluctuations in tail length among a population of many chains. The normalization of the distribution remains of order unity for $\tau \ll \tau_N$.

order N . Assuming for the moment that this continues to be true for all times, one has from equation (21)

$$\frac{dD_\tau(s)}{d\tau} \approx \frac{Q}{s^\nu} \quad (s_\tau^{\max} \ll s \ll N), \quad (25)$$

which after integration gives

$$\omega_\tau(s) \approx \frac{1}{s_\tau^{\max}} \left(\frac{s_\tau^{\max}}{s} \right)^{1+\nu} \quad (s_\tau^{\max} \ll s \ll N). \quad (26)$$

Thus, the first loops which form have the same loop distribution profile as the small s behavior of $k(s|N)$. However, the validity of equation (26) is limited to $s > s_\tau^{\max}$. This can be seen by substituting back equation (26) into equation (21), revealing that the assumption that only tails contribute to the rhs of equation (21) is incorrect for $s \lesssim s_\tau^{\max}$. This limits the validity of equation (26) to those loop sizes too great to have been formed by tail collapse events by the time τ . This is reflected by the fact that the integral of equation (26) in its region of validity is of order unity and dominated by s of order s_τ^{\max} .

Now for $s < s_\tau^{\max}$, the main body of the loop distribution, we seek a quasi-static solution, $dD_\tau/d\tau \approx 0$, or equivalently from equation (21),

$$\int_s^N ds' \lambda(s|s') \omega_\tau(s') \approx 0 \quad (1 \ll s \ll s_\tau^{\max}), \quad (27)$$

representing the expectation that such loops reach a self-maintained universal distribution. We show in Appendix D that equation (27) has a power law solution:

$$\omega_\tau(s) \approx \frac{1}{s_\tau^{\max}} \left(\frac{s_\tau^{\max}}{s} \right)^{2-\nu} \quad (1 \ll s \ll s_\tau^{\max}). \quad (28)$$

The normalization of equation (28) was fixed by demanding continuity with equation (26) at s_τ^{\max} . Combining

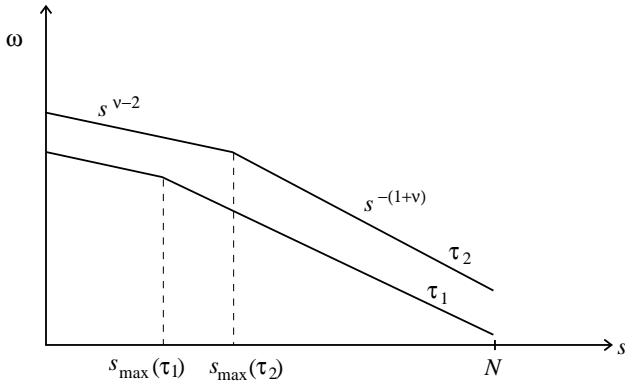


Fig. 8. Log-Log plot of single-chain loop distribution $\omega_\tau(s)$ for chemisorption from dilute solutions at two different times, $\tau_1 < \tau_2$. The distribution consists of an inner and an outer region with $\omega \sim s^{-7/5}$ and $\omega \sim s^{-8/5}$, respectively, for good solvents ($\nu = 3/5$). Both the normalization, which is equal to the total number of loops, and the size of the inner region increase with time. The outer region extends up to s of order $N - s^{\max}$. For larger s , the distribution is shown in Figure 7 describing the size of the large tail.

equation (28) and equation (26) we obtain the overall loop distribution shown in Figure 8.

Now the remaining part of the loop profile is the particular contribution due to trains. That is, we must still calculate the total number of adsorbed chain units $\gamma_{\text{bound}}(\tau)$. One might think this is just $\omega(1)$, the number of minimal length loops. This is wrong because there is in fact a sink for loops of length 1, *i.e.* a current out of the $\omega(s)$ distribution into the total mass of trains, $\gamma_{\text{bound}}(\tau)$. The latter obeys the dynamics of equation (19) but with the decay term deleted since bound monomers cannot decay into smaller ones:

$$\frac{d\gamma_{\text{bound}}}{d\tau} \approx 2 \int_1^\infty ds' \omega_\tau(s') k(s|s') \approx Q^{-1} L(\tau). \quad (29)$$

Here, unlike equation (19), we used an explicit cutoff at $s = 1$. In the last expression of equation (29) we used the definition of the total number of loops, $L(\tau)$, and took into account that the integral is dominated by its lower limit. Thus equation (29) reduces to equation (16) leading to the solution of equation (14).

In summary, using $\nu = 3/5$, our results for single-chain chemisorption are

$$\gamma_{\text{bound}}(\tau) \approx \begin{cases} (Q\tau)^{5/3} & (\tau < \tau_N), \\ N & (\tau > \tau_N), \end{cases}$$

$$\omega_\tau(s)s_\tau^{\max} \approx$$

$$\begin{cases} (s_\tau^{\max}/s)^{7/5} & (1 < s < s_\tau^{\max}), \\ (s_\tau^{\max}/s)^{8/5} & (s_\tau^{\max} < s < N), \\ [s_\tau^{\max}/(N-s)]^{8/5} h(s_\tau^{\max}/(N-s)) & (s \rightarrow N), \end{cases} \quad (30)$$

where

$$\tau_N \approx Q^{-1} N^{3/5}, \quad s_\tau^{\max} \approx (Q\tau)^{5/3}, \quad (31)$$

and the expression for ω_τ is for $\tau < \tau_N$. A schematic of the loop distribution is shown in Figures 6, 7, and 8. Apart from extra details, these results are identical to the ones we obtained in Section 3.2, equation (18), using scaling arguments. Analogous results to equation (30) can be obtained for theta solvents replacing $\nu \rightarrow 1/2$ in all expressions of this section.

4 Chemisorption: kinetics of polymer layer formation

In this section we consider the full chemisorption process where many chains simultaneously attach to the surface as in Figure 1. Initially, this is a simple superposition of single-chain adsorption processes discussed in Section 3. As chains build up and overlap, this becomes a many-chain phenomenon. We will determine the kinetics of total and surface-bound mass per unit area, $\Gamma(t)$, and $\Gamma_{\text{bound}}(t)$, the relationship $\Gamma_{\text{bound}}(\Gamma)$, the monomer density profile $c(z)$, and the internal structure of the layer characterized by the loop distribution per site, $\Omega(s)$. Finally, we determine the distribution of fraction of adsorbed monomers per chain, $P(f)$. We explicitly set $\nu = 3/5$ and it will be convenient to reinstate explicit reference to the monomer size a , hitherto set to unity.

4.1 Monolayer forms at early stages

In the early stages of adsorption, surface-attached chains are dilute on the surface and each one performs its accelerated zipping-down in a time τ_N . Thus, the layer is a superposition of such chains which arrived on the surface at different times, the structure of each being given by equation (30). Now the rate of chain arrival onto the surface is $a^2 d\Gamma/dt = QN\phi_{\text{surf}}$, where Γ is monomers per unit area and ϕ_{surf} is the equilibrium monomer density at the surface:

$$\phi_{\text{surf}} = \phi_{\text{bulk}} \frac{Z_{\text{surf}}(N)}{Z_{\text{bulk}}(N)} = \frac{\phi_{\text{bulk}}}{N}. \quad (32)$$

Here Z_{surf} , Z_{bulk} are the single-chain partition functions given a monomer on the surface or in the bulk, respectively. Their ratio has been shown to be $1/N$ in reference [77]. Solving for the kinetics one thus obtains

$$\Gamma(t)a^2 = \phi_{\text{bulk}} Qt, \quad t < t_{\text{sat}}^{\text{chem}} \equiv 1/(Q\phi_{\text{bulk}}), \quad (33)$$

where $t_{\text{sat}}^{\text{chem}}$ is the timescale at which $\Gamma \approx 1/a^2$, *i.e.* when surface density is of order one monomer per “site” of area a^2 . Clearly, as $t_{\text{sat}}^{\text{chem}}$ is approached, the kinetics of equation (33) should be drastically modified to take into account the depletion of available landing sites for new chains.

Notice that $\Gamma(\tau_N)/N \approx (\phi_{\text{bulk}}/\phi^*)/R_F^2$, where $\phi^* = N^{-4/5}$ is the chain overlap threshold concentration [79]. Thus for dilute solutions, $\phi_{\text{bulk}} < \phi^*$, attached chains are dilute on the surface at time τ_N , the necessary time for

a chain to fully adsorb. At any moment, therefore, those chains actually in the process of chemisorption are dilute on the surface and so do not interfere with one another's adsorption process. Chains adsorb *independently*. (Note that for higher concentrations, *i.e.* for ϕ_{bulk} in the semidilute regime, chain interference effects would be important and the resulting layers different.)

Although a given adsorbing chain does not see *simultaneously* adsorbing chains, in the later stages of layer formation it will be affected by those which have *previously* adsorbed, because these diminish the available empty surface sites. This effect becomes strong after time $t_{\text{sat}}^{\text{chem}}$. Some interference of this type will commence at an earlier stage, when flattened down adsorbed chains first start to overlap on the surface. This happens at coverage $\Gamma = N/R_F^2 \approx N^{-1/5}a^2$, which occurs after time $t_{\text{overlap}} \approx t_{\text{sat}}^{\text{chem}}N^{-1/5}$. This is initially a very small effect, since at time t_{overlap} the fraction of unavailable sites is small for large N , of order $N^{-1/5}$, so the essential features of the adsorption kinetics will remain unmodified. This becomes an order unity effect only at $t_{\text{sat}}^{\text{chem}}$. Between the two times, there is a continuously increasing interference. However, for practical values of N this is such a weak power that the timescales t_{overlap} and $t_{\text{sat}}^{\text{chem}}$ will be difficult to distinguish. (In fact for theta solvents, $\nu \rightarrow 1/2$, the two timescales become the same.)

Now the bound component of the attached chains of equation (33) is a sum over the bound mass of each chain which depends on the time it arrived on the surface: $\Gamma_{\text{bound}}(t) = \int_0^t dt' \Gamma(t') \gamma_{\text{bound}}(t - t')/N$. Using equations (33) and (30), one thus has

$$\begin{aligned} \Gamma_{\text{bound}}(t)a^2 \approx & \\ \begin{cases} \phi_{\text{bulk}} Q N^{3/5} (t/\tau_N)^{8/3} & (t < \tau_N), \\ \phi_{\text{bulk}} Q t & (\tau_N < t < t_{\text{sat}}^{\text{chem}}). \end{cases} \end{aligned} \quad (34)$$

The short-time kinetics of equations (33) and (34) are schematically shown in Figure 11 below. One sees two regimes in the short-time behavior of Γ_{bound} which are also reflected in two regimes of $\Gamma_{\text{bound}}(\Gamma)$. From equations (33) and (34) one has

$$\Gamma_{\text{bound}} = \begin{cases} \Gamma(\tau_N)[\Gamma/\Gamma(\tau_N)]^{8/3}, & \Gamma < \Gamma(\tau_N), \\ \omega \Gamma, & \Gamma(\tau_N) < \Gamma < a^{-2}. \end{cases} \quad (35)$$

This early portion of the $\Gamma_{\text{bound}}(\Gamma)$ curve is illustrated in Figure 2(a). In equation (35) we explicitly introduced the proportionality prefactor ω . This is a small-scale species-dependent constant representing the fact that even for isolated chains, steric constraints at the monomer level prevent every monomer from bounding. Thus, ω is the fraction of monomers which are allowed by such constraints to bound.

In summary, during the early stages of chemisorption, chains flatten out on the surface uninhibited by the presence of others. For very short times, $t < \tau_N$, none of the attached chains has completed its adsorption and the layer's loop distribution is a superposition of single-chain loop structures given by equation (30), summed over different

arrival times $t - \tau$. For times longer than τ_N , essentially all attached chains have fully adsorbed and a monolayer of flattened chains starts to develop, which at times of order $t_{\text{sat}}^{\text{chem}}$ has almost covered the surface.

Up to $t_{\text{sat}}^{\text{chem}}$, the fraction f of bound monomers is approximately the same for all chains and equal to ω . Thus $P(f)$ during this stage is sharply peaked at ω . In reality, we expect two types of effects will somewhat broaden this distribution. The first is fluctuations in f values around ω due to random events typical of multiplicative random processes characterizing irreversibility (*e.g.*, monomers trapped in knots might not be able to bind to the surface). Such fluctuations would be interesting to characterize numerically following the example of reference [69] in which a Monte Carlo method was used to study the structure of a single fully collapsed chain on a surface and an ω value was extracted using $\gamma_{\text{bound}} \sim \omega N$ for large N . We anticipate a second source of broadening for chains arriving after t_{overlap} . These chains will have f values which decrease with time since some monomers will be unable to bind due to the presence of earlier arrivers. This would lead to a continuously broadening spectrum of f values with increasing time. In practice, this overlap time is often close to the saturation time (*e.g.*, for $N = 1000$, $t_{\text{overlap}} = .25t_{\text{sat}}^{\text{chem}}$) so this broadening effect has little time to develop.

4.2 Late stages: diffuse outer layer

As the surface density approaches saturation, $a^2 \Gamma_{\text{bound}} \approx 1$, the availability of surface sites on the surface becomes scarce and the late-coming chains cannot fully adsorb on the surface as the early arrivers did. Let us suppose that the establishment of one surface attachment requires an empty spot large enough to accommodate n_{cont} bound monomers, where n_{cont} is a small-scale species-dependent number similarly to ω . The surface density of these "supersites," ρ_{super} , is becoming smaller with time and the mean separation, l_{sep} , between neighboring supersites increases accordingly, $l_{\text{sep}} \approx \rho_{\text{super}}^{-1/2}$. Now in order for late-coming chains to adsorb onto these surface spots, they have to form loops joining up these sites as shown in Figure 9. We model the adsorption of chains at these late stages by assuming that the size s of such loops is the equilibrium subcoil size corresponding to l_{sep} , *i.e.*

$$as^{3/5} = l_{\text{sep}} = \rho_{\text{super}}^{-1/2}. \quad (36)$$

Thus chains which adsorb at the instant when the typical loop size in equation (36) is s , have a fraction of bound monomers given by

$$f = \frac{\partial \Gamma_{\text{bound}}}{\partial \Gamma} = \frac{n_{\text{cont}}}{s}. \quad (37)$$

Now as Γ_{bound} approaches its asymptotic value, $\Gamma_{\text{bound}}^\infty$, which is another non-universal small-scale-dependent quantity of order a^{-2} , then

$$\Delta \Gamma_{\text{bound}} = n_{\text{cont}} \rho_{\text{super}} = n_{\text{cont}} \frac{a^{-2}}{s^{6/5}}, \quad (38)$$

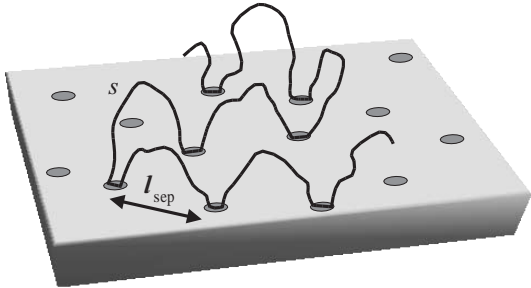


Fig. 9. Typical configuration of adsorbed chain at late stages of adsorption. Such chains can adsorb only onto free empty sites (shown as gray discs) which are separated by l_{sep} . They thus form loops of s monomers, with $as^{3/5} = l_{\text{sep}}$.

where $\Delta\Gamma_{\text{bound}} \equiv \Gamma_{\text{bound}}^\infty - \Gamma_{\text{bound}}$ and we used equation (36). Equation (38) is simpler to understand starting from the completely saturated surface: it states that if one were to unpeel chains from a completely saturated surface so as to create ρ_{super} supersites, the number of bound monomers freed would be n_{cont} per supersite.

Now integrating equation (37) after using equation (38), one has

$$a^2 \Delta\Gamma_{\text{bound}} = n_{\text{cont}} (a^2 \Delta\Gamma / 6)^6, \quad (39)$$

which together with equation (35) of the early stages describe the full theoretical relation between bound and total fractions plotted in Figure 2(a). Thus equation (39) predicts a very sharp saturation of the bound fraction as $\Gamma \rightarrow \Gamma^\infty$.

Now since in our picture every point along the $\Gamma_{\text{bound}}(\Gamma)$ curve corresponds to a unique value of f , see equation (37), then the weighting of f values is given by

$$\begin{aligned} P(f) &= \frac{1}{\Gamma^\infty} \int d\Gamma \delta(f - \partial\Gamma_{\text{bound}}/\partial\Gamma) \\ &= \frac{1}{\Gamma^\infty} \left(\left| \partial^2\Gamma_{\text{bound}}/\partial\Gamma^2 \right|_{\partial\Gamma_{\text{bound}}/\partial\Gamma=f} \right)^{-1}, \end{aligned} \quad (40)$$

which after using equation (39), leads to

$$P(f) = Cf^{-4/5} \quad (f \ll 1) \quad (41)$$

with $C \approx 6/(5a^2\Gamma^\infty[n_{\text{cont}}]^{1/5})$.

The full theoretical prediction for the final layer's distribution of f values is thus the sum of equation (41) and a sharply peaked function at ω from the early stages. The overall distribution is shown in Figure 2(b), binned into bins of width $\Delta f = 0.02$. The binned distribution exhibits 2 peaks, of different origin: the peak at large f corresponds to early-arriving chains and its position is species dependent, while the peak at $f = 0$ represents a diffuse outer layer shown in Figure 10 and is due to the universal small f form, $P(f) \sim f^{-4/5}$.

Let us consider now the distribution of loop sizes in the resulting diffuse layer, $\Omega(s)$, equal to the number of loops of length s per unit area per unit loop length. This may be found by noting that the bound mass corresponding to a certain $d\Gamma_{\text{bound}}$ has a unique s value and must thus equal

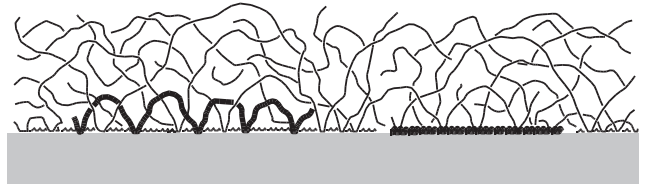


Fig. 10. Sketch of predicted final layer structure resulting from irreversible polymer adsorption. The layer consists of two parts (one chain from each part is highlighted): i) An inner region of flattened down chains making ωN contacts per chain, where ω is of order unity. ii) A diffuse outer layer build-up from chains each making $f N \ll N$ contacts with the surface. The values of f follow a distribution $P(f) \sim f^{-4/5}$. Each f value corresponds to a characteristic loop size for a given chain, $s \approx n_{\text{cont}}/f$.

the bound mass in loops of length s , namely $n_{\text{cont}}\Omega(s)ds$. Using equation (38) this leads to

$$\Omega(s) \approx a^{-2}s^{-11/5}. \quad (42)$$

What density profile $c(z)$ does this loop distribution generate as a function of distance z from the surface? To determine the density profile, we follow similar arguments to those of references [13–15] which relate loop distributions to density profiles in both specific and general cases. We do that by assuming that the density at a given height z is due to contributions from loops longer than $\sigma(z)$, where σ is the loop length which extends spatially up to height z . The density at a given height is determined by the number of loops which are long enough to reach this height:

$$c(z) \approx \frac{d\sigma(z)}{dz} \int_{\sigma(z)}^{\infty} ds \Omega(s). \quad (43)$$

Since in our case loops are not stretched, one has $z \approx a\sigma^{3/5}$. Thus using equation (42) in equation (43) one obtains the algebraic profile,

$$c(z) \approx c(a) \left(\frac{a}{z} \right)^{4/3}, \quad (44)$$

which interestingly has the same scaling form as de Gennes' self-similar profile of equilibrium polymer layers [10].

Let us finally consider the *kinetics* of the building-up of the diffuse layer. Since the rate of attachment is proportional to the density of available surface sites, the early kinetics of equation (33) generalize to

$$\frac{d\Gamma}{dt} = \phi_{\text{bulk}} Q \Delta\Gamma_{\text{bound}}. \quad (45)$$

(In Eq. (45) we did not include free-energy barriers due to loops of the already partially formed layer which would present excluded-volume repulsion to new chains arriving at an empty supersite. In fact, in order for our picture to be self-consistent, such effects must be very small; were there any dangling loops near an empty supersite they would adsorb onto this site.) Thus from equation (45) one has

$$\begin{aligned} a^2 \Delta\Gamma &\approx F (t_{\text{sat}}^{\text{chem}}/t)^{1/5}, \\ a^2 \Delta\Gamma_{\text{bound}} &\approx G (t_{\text{sat}}^{\text{chem}}/t)^{6/5} \quad (t > t_{\text{sat}}^{\text{chem}}), \end{aligned} \quad (46)$$

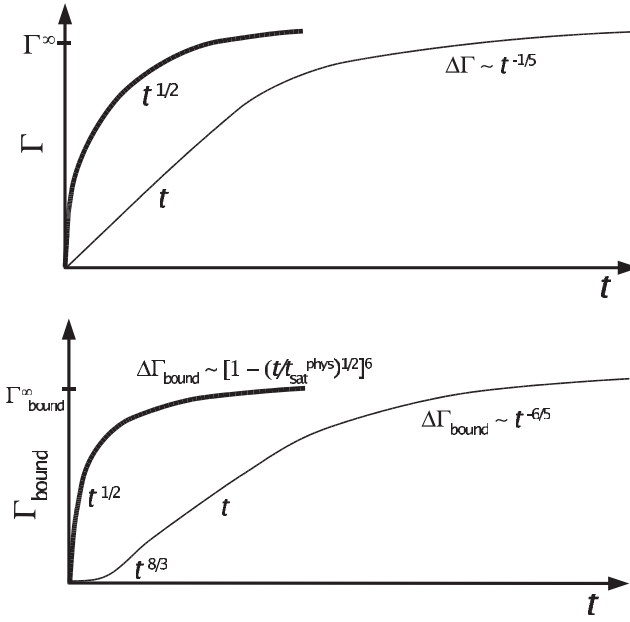


Fig. 11. Time evolutions of total, Γ , and surface bound, Γ_{bound} , monomers per unit area, as a function of time, as predicted by theory. Both chemisorption (thin lines) and physisorption (thick lines) are sketched. The total mass for chemisorption grows initially linearly, $\Gamma \sim t$, and then slows down as the surface saturates, $\Delta\Gamma \equiv \Gamma^\infty - \Gamma \sim t^{-1/5}$. For physisorption $\Gamma \sim t^{1/2}$ has diffusion-controlled form for all times until saturation. The surface-bound part for chemisorption undergoes three regimes: initially $\Gamma_{\text{bound}} \sim t^{8/3}$, crossing over to $\Gamma_{\text{bound}} \sim t$ and then to the late-stage saturation behavior, $\Delta\Gamma_{\text{bound}} \sim t^{-6/5}$. The surface-bound part for physisorption follows initially diffusion-controlled kinetics, $\Gamma_{\text{bound}} \sim t^{1/2}$, but for longer times the kinetics slow down, $\Delta\Gamma_{\text{bound}} \equiv \Gamma_{\text{bound}}^\infty - \Gamma_{\text{bound}} \sim [1 - (t/t_{\text{sat}}^{\text{phys}})^{1/2}]^6$.

after using equation (39). The prefactors $F = 6(5n_{\text{cont}}/6)^{-1/5}$, $G = n_{\text{cont}}(C/6)^6$ are close to unity. Together with the short-time kinetics, equations (33) and (34), these evolutions are sketched in Figure 11.

So far in this section good-solvent conditions were assumed. Generalizing to the case of theta solvents is straightforward, by replacing $\nu = 3/5 \rightarrow 1/2$. One finds qualitatively similar results with $\Delta\Gamma_{\text{bound}} \sim e^{-\Gamma a^2}$ replacing equation (39), and the distribution of bound fractions is now $P(f) \sim f^{-1}$, replacing equation (41).

5 Irreversible physisorption

We consider now the other important class of irreversible adsorption: strong physisorption. In this case, monomer-surface bonds form immediately upon contact and adsorption kinetics are diffusion-controlled. Despite the completely different kinetics compared to chemisorption, we find the resulting polymer layers have nevertheless almost identical structure.

5.1 Early stages: monolayer formation

Initially, the surface is empty and it is thus inevitable that any chain whose center of gravity diffuses within the coil size [79, 81] $R_F = aN^{3/5}$ of the surface will adsorb. Thus attachment of chains is diffusion-controlled and the surface coverage grows as

$$a^2\Gamma(t) \approx \frac{\phi_{\text{bulk}}}{a} (Dt)^{1/2}, \quad (47)$$

where D is the chain center-of-gravity diffusivity.

Consider now the part of adsorbed mass which has bonded with the surface, Γ_{bound} . Immediately after the first attachment, the subsequent monomer arrivals on the surface occur at the rate of their diffusion on the surface. Imagine there were no reactions and that the surface was a penetrable plane. Then, given the coil is initially next to the surface, all monomers would cross the plane at least once within the bulk coil relaxation time τ_{bulk} [79, 81]. With reactions turned on, each time a monomer reaches the plane, it would react with it. We expect the effect of the resulting constraint to further accelerate the rate of a new monomer arrival onto the surface and thus the chain physisorption time τ_{ads} would be at most τ_{bulk} . We do not attempt to analyze the details of these kinetics involving polymer hydrodynamics with increasing number of constraints. Such kinetics would anyway be very difficult to detect experimentally since typical coil relaxation times in solution are microseconds. Here, it is enough to know that $\tau_{\text{ads}} \lesssim \tau_{\text{bulk}}$, which is supported by numerical simulations in the absence of hydrodynamic interactions in reference [70]. Thus provided the solution is dilute, $\phi < \phi^*$, each chain adsorbs fast enough onto the surface before other chains interfere with it.

Since the single-chain adsorption time is faster than new chain arrival on the surface, a monolayer of flattened chains starts to develop on the surface, just as in the case of chemisorption. Defining ω to be the surface-bound part of a completely collapsed chain, as in chemisorption, we thus have

$$\Gamma_{\text{bound}} = \omega\Gamma, \quad (48)$$

This is the initial linear regime in Figure 2(a).

The kinetics of equation (47) proceed up to a time at which the density of available surface sites starts to become small, *i.e.* when $\Gamma \approx a^{-2}$. This occurs at a time of order

$$t_{\text{sat}}^{\text{phys}} \approx \tau_{\text{bulk}} \left(\frac{\phi^*}{\phi_{\text{bulk}}} \right)^2 N^{2/5}. \quad (49)$$

After this time, new chains must form loops joining disconnected empty sites and a diffuse layer starts to build up.

5.2 Late stages: diffuse outer layer

For times longer than $t_{\text{sat}}^{\text{phys}}$, the late-coming chains start to see a continuously decreasing density of available sites for adsorption. Will the adsorption kinetics continue to be diffusion-controlled? Consider a chain which was brought

by diffusion to within one coil size R_F of the surface. Let us see if a bond forms before it diffuses away. The number of collisions the chain makes with a certain site on the wall within R_F of its center of gravity before it diffuses away is

$$N_{\text{coll}} \approx (\tau_{\text{bulk}}/t_a) N_{\text{site}}, \quad N_{\text{site}} \approx r \frac{Na^3}{R_F^3}. \quad (50)$$

Here t_a is the monomer relaxation time and N_{site} is the mean number of the coil's monomers per surface site within the coil's projected surface area. This would simply be of order Na^3/R_F^3 , but the presence of the hard wall reduces it by a factor $r \equiv Z_{\text{surf}}(N)/Z_{\text{bulk}}(N) = 1/N$ as in equation (32). Using [79, 81] $\tau_{\text{bulk}} \approx t_a(R_F/a)^3$, one has from equation (50)

$$N_{\text{coll}} \approx 1. \quad (51)$$

Thus the chain makes of order one surface contact with every site on the surface within the coil size. It follows that unless the surface density of available sites is so small as to be of order one per R_F^2 , it is inevitable that during the chain's residence time on the surface at least one monomer-surface bond will form. Thus the diffusion-controlled kinetics of equation (47) continue up to the point where essentially every empty site is filled.

What is the mode of adsorption of these late-coming chains which attach to the few empty sites? We model adsorption in these late stages in a similar way to the build-up of the diffuse outer layer in chemisorption (Sect. 4.2). The late-coming chains, after adsorbing on an empty site large enough to accommodate n_{cont} monomers, form bridges to nearby empty sites which are loops of s monomers when the average separation between neighboring empty sites is $l_{\text{sep}} \approx as^\nu$ (see Fig. 9). This separation becomes larger as more and more chains adsorb. Thus the diffuse layer density profile $c(z)$, distributions of loop sizes, $\Omega(s)$, and distribution of fraction of adsorbed monomers per chain, $P(f)$, are the same as for chemisorption (Sect. 3). Including the monolayer contribution due to short times, the resultant overall $\Gamma_{\text{bound}}(\Gamma)$ and $P(f)$ relations are plotted in Figure 2. This is a repeat of the chemisorption curves with the exception of the early $\Gamma_{\text{bound}} \sim \Gamma^{8/3}$ regime exclusive to chemisorption. The sketch of the resulting polymer layer is the same as Figure 10.

The major distinction between chemisorption and physisorption arises in the kinetics of layer build-up. The difference in the $\Gamma(t)$ kinetics is evident by comparing equation (47) for physisorption, valid up to complete surface saturation, to equations (33) and (46) for chemisorption. Similarly, the kinetics of the bound fraction, Γ_{bound} are also very different. For physisorption, the short-time kinetics are given by substituting equation (47) in equation (48) while the long-time behavior is found using equation (47) in equation (39), leading to

$$a^2 \Delta \Gamma_{\text{bound}} \approx \begin{cases} \omega \phi_{\text{bulk}} a^{-1} (Dt)^{1/2} & (t \ll t_{\text{final}}^{\text{phys}}), \\ n_{\text{cont}} (a^2 \Gamma^\infty)^6 \left[1 - (t/t_{\text{final}}^{\text{phys}})^{1/2}\right]^6 & (t \rightarrow t_{\text{final}}^{\text{phys}}). \end{cases} \quad (52)$$

Here $t_{\text{final}}^{\text{phys}}$ is the complete surface saturation time, after which the diffuse layer has completely formed. This timescale is of the same order of magnitude as $t_{\text{sat}}^{\text{phys}}$ since the surface coverage of the outer layer, $\int_a^{R_F} dz c(z) \approx a^{-2}$, is of the same order as the monolayer coverage. Thus from equation (47) one sees that the time for diffuse layer formation is of the same order as the time of monolayer formation since both require the diffusion to the surface of about the same quantity of mass. The complete evolution of $\Gamma(t)$ and $\Gamma_{\text{bound}}(t)$ is sketched in Figure 11.

6 Discussion

6.1 Comparison of theory with experiment

We studied theoretically the structure of polymer layers formed by irreversible adsorption onto surfaces from dilute solution under good- or theta-solvent conditions. Relatively few theoretical works have addressed irreversibility in polymer adsorption. In references [67, 68], irreversible physisorption was studied analytically and numerically within the framework of self-consistent mean-field theory. These workers found that, compared to equilibrium, the irreversibly formed layers are different in that i) the asymptotic surface coverage Γ^∞ was larger in equilibrium, and ii) in the irreversible case the density profile $c(z)$ was found to be larger for small and large z , but smaller for intermediate values as compared to equilibrium. In another work [46], single-chain chemisorption of PMMA onto Al was studied by solving numerically the loop kinetics, equation (19), using chain statistics corresponding to theta-solvent solutions. It was found that the chain adsorbs in a zipping mechanism the origin of which was greatly enhanced reactivities for monomers neighboring a graft point. These reactivities were taken as greatly enhanced on the basis of electronic structure calculations [82, 83].

In this work the cases of irreversible physisorption and chemisorption were examined separately. We found that in both cases the final layer consists of two regions. In an inner region of completely flattened chains, each chain has on average ωN monomers bound to the surface. The value of ω is species dependent and represents the effect of steric constraints at the monomer level which prevent all monomers of the chain from bonding. The outer region is a tenuously attached diffuse layer of chains making $fN \ll N$ contacts with the surface. The distribution of f values among chains is universal and in a good solvent follows $P(f) \sim f^{-4/5}$ for $f \ll 1$. This double-layer structure is illustrated in Figure 10 which exhibits two peaks at small and large f , respectively. Our theory cannot capture the numerical value of the peak amplitude near $f = \omega$, but the existence of a peak (or possibly of a depletion region) is due to small-scale effects. The first layer of flattened chains is special because these arrive at a bare surface, and chain features on the scale of a monomer size are involved. In our picture, one can think of the next set of arriving chains (which are just starting to build up the outer tenuously attached region) as seeing a different surface, one containing a certain areal fraction of empty sites

less than unity. This set cannot flatten down completely. The third set of arriving chains sees a surface containing a yet lower density of free sites, and so on. For large layer numbers, a chain sees a universal surface whose features evolve self-similarly with increasing layer number. This leads to a universal power law form for $P(f)$. Returning to the earliest layers, these are formed before universality onsets, reflected in a non-universal feature in $P(f)$ near $f = \omega$.

Using infrared absorption spectroscopy, measurements of $P(f)$ for irreversible physisorption of PMMA onto oxidized silicon have been pioneered in the experiments of references [31–33], measurements from which are reproduced in Figure 2(b). In this figure, the theoretical prediction is compared to experiment by binning values in ranges $\Delta f = 0.02$ and converting analytical predictions to a histogram. Since $f = 0.08$ is the lowest observed experimental value, we cut off the theoretical distribution at the same point for the sake of comparison. The contribution from the inner layer is represented by a delta-function centered at $\omega \approx 0.47$, though as discussed in Section 4, we expect this to be broadened. We see that the agreement with experiment is good and captures the bimodal shape of the distribution. We note that measuring lower f values to see a clear signature of a power law regime may be difficult: our theory suggests these chains are a small fraction of the total chain population (the integral of $P(f)$ is dominated by large f). However, since those chains lie in the outermost region of the layer, they would determine important physical properties such as hydrodynamic thickness and the strength of interaction of the polymer layer with an approaching interface. In comparing with theory above, we have used our predictions for good solvents. However, the experiments of references [31, 32] were performed under solvent conditions slightly better than theta. Thus, it may be that a more appropriate comparison is with our theory specialized to theta solvents, for which the predicted $P(f) \sim 1/f$ is very similar.

The building-up of the double layer is apparent in the shape of $\Gamma_{\text{bound}}(\Gamma)$ where Γ_{bound} , Γ , are the surface-bound and the total surface coverage, respectively. For irreversible physisorption we found that initially $\Gamma_{\text{bound}} \approx \omega\Gamma$. As the surface saturates, the diffuse layer starts to develop and $(\Gamma_{\text{bound}}^\infty - \Gamma_{\text{bound}}) \sim (\Gamma^\infty - \Gamma)^6$ as the asymptotic values (denoted by ∞) are approached which are of order a^{-2} , where a is the monomer size. We thus predict a very sharp saturation of the bound fraction as Γ saturates; the resulting curve is plotted in Figure 2(a). A very similar curve has been measured in the experiments discussed in the previous paragraph [31, 32], where the initial slope was $\omega \approx 0.47$, the value we used in Figure 2(b). In addition the shape of the curve was found to be independent of chain length, which is also consistent with our model. For chemisorption, the curve is similar but we predict an additional $\Gamma_{\text{bound}} \sim \Gamma^{8/3}$ regime as shown in Figure 2(a).

Contrary to physisorption, the experimental picture for chemisorption is much less clear, though since time-scales are intrinsically much longer, the kinetics might be easier to probe. Experiments on various systems have been

performed [44, 45, 48, 84–86] the results of which, however, cannot be interpreted within the framework of our present theory since they involved simultaneous physisorption and chemisorption. In certain cases the degree of polymer functionalization was also varied [44, 45, 84]. Clearly, the dependence of resulting polymer structures on degree of polymer or surface functionalization is an interesting aspect deserving further study.

This paper has addressed both the structure of the final layer and the irreversible kinetics of its formation. Chemisorption kinetics are very slow and are chemically controlled. We found that initially $\Gamma \sim t$, followed by $\Gamma \sim t^{-1/5}$ as the surface saturates. We remark that for long enough times, adsorption onto a planar surface always becomes diffusion-controlled after a Q -dependent timescale [87, 88], where Q is the reaction rate upon monomer-surface contact. Here our assumption is that Q is small enough such that this cross-over time is very large, which is the typical case for ordinary chemical species. For physisorption, diffusion-controlled kinetics apply until saturation, $\Gamma \sim t^{1/2}$. The corresponding time dependencies for Γ_{bound} follow from $\Gamma_{\text{bound}}(\Gamma)$ and are shown in Figure 11.

A large part of this work has focused on single-chain chemisorption. Unlike physisorption, where single-chain adsorption is complete at most after the coil's bulk relaxation time, τ_{bulk} , we found that the adsorption time in chemisorption is much larger, $\tau_{\text{ads}} \approx Q^{-1}N^{3/5}$. Thus, for typical $Q \approx 1 \text{ s}^{-1}$, $N = 1000$, one has $\tau_{\text{ads}} \approx 60 \text{ s}$, a time accessible to experimental measurements. During τ_{ads} the chain adsorbs onto the surface in a mode we call accelerated zipping: initially, the chain adsorbs in a zipping mechanism growing outwards from the first attachment point with the surface, but with increasing time distant monomers adsorb forming large loops and new sources for further zipping which accelerate the chain's collapse. The distribution of these loop sizes follows a power law $\omega(s) \sim s^{-7/5}$ while the number of bound monomers grows as $\gamma_{\text{bound}}(t) \sim t^{5/3}$.

6.2 Differences between irreversible and equilibrium layers

We conclude with a general comparison between the final non-equilibrium layers predicted by our theory and equilibrium layers. This discussion is limited to good solvents. Our results for the final loop distribution of the layer, $\Omega(s) \sim s^{-11/5}$ and density profile $c(z) \sim z^{-4/3}$ have interestingly identical scaling form to the corresponding equilibrium results. On the other hand, the configurations of individual chains are very different. In the equilibrium layer a given chain has $ND(s)$ loops of length s or greater, where $D(s) \equiv \int_s^\infty ds' \Omega(s') \sim s^{-6/5}$. Because of screening effects, these are essentially independent blobs and their 2D spatial extent parallel to the surface is $[ND(s)]^{1/2}as^{3/5} = aN^{1/2}$. This is true for all scales s ; in particular, there is order one loop of length $N^{5/6}$, also of size $aN^{1/2}$. Hence a typical chain has a size [6] of order $aN^{1/2}$, the ideal result (to within logarithmic

corrections [6]). Chains in the non-equilibrium layer are by contrast of size $aN^{3/5}$, due to the adsorption kinetics which in the case of chemisorption entailed occasional adsorption of very large loops of length N , which ensured the final state of the chain extends a distance of order $aN^{3/5}$ parallel to the surface. We did not attempt to unravel the complex details of physisorption, but our assumption was that the 3D coil ends up being roughly projected onto the 2D surface, leading again to a lateral size $aN^{3/5}$.

The most fundamental distinguishing feature of the non-equilibrium layer is that different chains have different loop distributions and fractions of adsorbed segments, f , which are frozen in time. There is no longer one single thermodynamic f . Instead, there are infinitely many classes of chains, each with its own f value, and the number of chains in each class is proportional to $P(f)$. Each chain has a characteristic loop size, $s \sim 1/f$.

This is very different to the equilibrium layer where all chains are statistically identical, in that every chain explores in time the same range of f values with the same relative weighting $P^{\text{eq}}(f)$. In fact, one can show that for large N this distribution P^{eq} is very sharply peaked at a mean value \bar{f} of order unity, with width of order $N^{-1/6}$. (The mean value is due to small loops of order unity while the fluctuations are due to the mass in very large loops with length of order $N^{5/6}$. Since there is order one such loop, this diminishes f by an amount of order $N^{-1/6}$.) Thus, even at any fixed moment in time it is still a true statement that almost all chains have the same f value, \bar{f} , to within fluctuations which are small for large enough N . We remark that there is a small population of chains, a fraction of order $N^{-1/5}$ of the total, with f values far removed from the mean: these are the chains with tails [15] of length of order N which determine the layer height $\approx aN^{3/5}$.

These differences in chain statistics between irreversible and equilibrium layers have important implications for various physical properties of the layer. Consider a physisorbing system whose surface relaxation kinetics are very slow, but not truly irreversible (we expect this is a rather common case). In this case for times of order the layer formation time we expect the layer is well described by the irreversible $P(f)$. For much longer timescales on which surface bonds are reversible, equilibration processes will slowly evolve $P(f)$ into $P^{\text{eq}}(f)$. Our picture predicts that during this process the total coverage, density profile, and loop distribution remain unchanged to within prefactors of order unity. Single-chain statistics will be significantly affected, however, and individual chains must shrink in order to occupy a much smaller region in space. This change is expected to profoundly modify the physical properties of the layer. For example, the fraction of chains with long loops and tails of order N will be reduced by a factor $N^{-1/5}$, thus strengthening the outer region of the layer which is exposed to the bulk. Similarly, in experiments probing the kinetics of exchange between chains in the bulk and those in the layer [24–30,33,36–39], we expect strong aging effects since the number of easily exchangeable, loosely attached chains is decreasing with increasing

aging time. This would lead to a decrease of the initial exchange rate with aging time as observed [28,29,37,38]. Further theoretical work is clearly needed to interpret the phenomenology of these experiments. One unexplained observation, for example, concerns poly(ethylene oxide) adsorption onto silica where the bulk-surface exchange rate of chain subpopulations in non-equilibrium layers has been measured to be independent of the time the subpopulation was incorporated in the layer [39].

What is the origin of the theoretically predicted irreversible layer's overall loop distribution being the same as that in equilibrium? This is rooted in the kinetics of our model. In the late stages, we assumed the equilibrium relation between loop size and number of monomers s in the loop, $R \sim s^\nu$. That is, a given loop is assumed to have equilibrium statistics. It is important to note that this does not by itself lead to the equilibrium loop distribution. Our basic assumption on the late-stage kinetics is that the kinetically selected loop size R at any moment is determined by the current density of free supersites, $\rho_{\text{super}} \sim 1/R^2$. Taken together with $R \sim s^\nu$, this then leads to the $\Omega(s)$ of equation (42). These kinetics are mean field in character, assuming uniformly smeared free sites determined by the current global value of ρ_{super} rather than any local feature. The correct choice of kinetics is governed by the kinetics of the chain adsorption process.

To illustrate this point, consider a general situation, involving chain adsorption onto a d -dimensional surface. Suppose the mechanism of adsorption is pure zipping and follow the process from a starting situation where the surface has a uniform density of empty surface sites, $\rho_{\text{super}} = l^{-d}$. Roughly speaking, such a zipping chain performs a simple random walk on the surface, each step filling one empty site and producing a loop of length $s = l^{1/\nu}$. The statistics of this process depend on dimensionality. i) Suppose $d = 1$. Since a 1D random walker explores space “compactly” [89], *i.e.* visits each site within its exploration volume many times, by the time the zipping is complete and the chain has fully adsorbed, a surface patch depleted of empty sites will have been created in the region where the chain has adsorbed. Later-arriving chains can then occupy only the empty regions between such patches created by previously adsorbed chains. We expect the density of free sites to fluctuate very strongly, invalidating any mean-field approach. ii) $d = 3$. The zipping process is now a “non-compact” random walk, occupying only a small fraction of the free-surface sites within its exploration volume. Fluctuations are small, and the mean-field approach which assumes an essentially uniform distribution of free sites of density ρ_{super} decreasing quasi-statically in time is valid. This is the assumption implicit in the present paper. iii) $d = 2$. Random walks are now marginally compact and one expects logarithmic corrections to the mean-field picture.

The situation treated in this paper is of course $d = 2$. Thus, one might expect logarithmic corrections to the loop distribution of equation (42) which had arrived at via the mean-field argument. In fact, for two reasons we expect the zipping process to execute a surface walk somewhat

expanded from a simple marginally compact 2D random walk. Firstly, no site can be adsorbed onto twice by the zipping random walk. Thus walks are repelled from frequently visited areas. This is a kind of self-avoidance, and one anticipates swelling of the walk somewhat similarly to the “true” self-avoiding walk [90] and the “kinetic growth” walk [91]. Secondly, the chain adsorption processes we have studied are not simple zipping. For chemisorption, the zipping is accelerated by occasional very large steps producing loops of all sizes up to N . These large excursions result in the flattened chain occupying an area of order $N^{6/5}$ rather than N . Since the fraction $N^{-1/5}$ of occupied sites within this area is small, one returns to a non-compact situation where mean field applies. In reality, this is over-simplified, since local zipping from nucleation points presumably involves correlations of the type characterizing pure zipping, so non-uniform depletion of empty sites may occur near zipping centers. For physisorption the process is even more complex, presumably involving a combination of local diffusion-mediated zipping and large loop formation, but one expects a projection area onto the surface again of order $N^{6/5}$ which naively suggests non-compact character.

From the above remarks, it is clear that stepping beyond our rather simple approach to irreversible adsorption involves many complex issues. We hope our work motivates future experiment and theory in this direction.

This work was supported by the National Science Foundation under grant no. DMR-9816374.

Appendix A. Single-chain chemisorption: interior monomers attach first

In this appendix we show that a single chain is much more likely to chemisorb on a surface by one of its interior monomers rather than with one of its ends. Consider the s -th monomer, where by definition s is the length of the shorter part of the chain, the other having length $N - s$. The reaction rate of this monomer with the surface is proportional to the partition function of the chain anchored by this monomer on the surface:

$$Z_{\text{cont}}(s) = \mu^N \eta(s/N) N^{\gamma_2 - 1},$$

$$\eta(x) \approx \begin{cases} x^{\gamma_2 - \gamma_1} & (x \ll 1), \\ 1 & (x \rightarrow 1/2), \end{cases} \quad (\text{A.1})$$

where μ is a constant of order unity. We derived $Z_{\text{cont}}(s)$ by demanding that i) it is a power in s and ii) in the limits $s \rightarrow 1$ and $s \rightarrow N/2$, one obtains the known partition functions $Z_{\text{cont}}(1) \approx \mu^N N^{\gamma_1 - 1}$, $Z_{\text{cont}}(N/2) \approx \mu^N N^{\gamma_2 - 1}$, respectively. The numerical values of γ_1, γ_2 are [6, 77, 78] $\gamma_1 \approx 0.68$, $\gamma_2 = \gamma - 1 \approx 0.16$, where γ is the susceptibility exponent [79].

Now the total rate for any monomer to react is proportional to $\int_1^{N/2} ds Z_{\text{cont}}(s)$. Since $\gamma_2 - \gamma_1 > -1$ this integral is dominated by large s . Hence it is much more likely for a monomer in the middle to be the first one to react

with the surface, rather than an end, roughly by a factor $N Z_{\text{cont}}(N)/Z_{\text{cont}}(1) \approx N^{1+\gamma_2-\gamma_1} \approx N^{0.48}$. Thus the accelerated zipping always propagates outwards from an interior monomer, as schematically illustrated in Figure 6.

Appendix B. Proof that equation (19) satisfies mass conservation

We show in this appendix that equation (19) conserves the total number of monomers $M^{\text{tot}} \equiv \int_0^\infty ds s \omega_\tau(s)$, by showing that $dM^{\text{tot}}/d\tau = 0$. This is equivalent to showing that the integral of the rhs of equation (19) over all positive s is zero. Changing variables from s' to $x = s'/s$ in the first term, and to $x = s'/s$ in the second term, on the rhs of equation (19), respectively, one has

$$2 \int_s^\infty ds' \omega_\tau(s') k(s|s') - \int_0^s ds' \omega_\tau(s) k(s'|s) =$$

$$\frac{2}{s^\nu} \int_0^1 dx \omega_\tau\left(\frac{s}{x}\right) \frac{\zeta(x)}{x^{1-\nu}} - \frac{\omega_\tau(s)}{s^\nu} \int_0^1 dx \zeta(x) \quad (\text{B.1})$$

after using equation (11). Multiplying equation (B.1) by s , integrating over all positive s and changing variables from s to $y = s/x$, one finds that the result vanishes by virtue of the identity $2 \int_0^1 dx x \zeta(x) = \int_0^1 dx \zeta(x)$ for $\zeta(x)$ symmetric around $x = 1/2$. Thus M^{tot} is conserved.

Appendix C. Derivation of equation (24) from equation (23)

Defining $\xi \equiv N - s$ and $\tilde{\omega}_\tau(\xi) \equiv \omega_\tau(N - \xi)$, one has from equation (23)

$$\frac{d}{d\tau} \int_0^\xi d\xi' \tilde{\omega}_\tau(\xi') = - \int_0^\xi d\xi' \frac{AQ \tilde{\omega}_\tau(\xi')}{(\xi - \xi')^\nu}. \quad (\text{C.1})$$

Laplace-transforming $\xi \rightarrow E$ (we allow ξ to take any positive value, *i.e.* we seek the $N \rightarrow \infty$ solution of Eq. (23)) one has from equation (C.1):

$$\frac{d}{d\tau} \tilde{\omega}_\tau(E) = -AQ E^\nu \tilde{\omega}_\tau(E), \quad (\text{C.2})$$

which after integration over τ becomes

$$\tilde{\omega}_\tau(E) = e^{-AQ\tau E^\nu}. \quad (\text{C.3})$$

We used the initial condition $\tilde{\omega}_0(E) = 1$, since $\omega_0(\xi) = \delta(\xi)$ (see Eq. (23)). Laplace-inverting [92] equation (C.3), one recovers equation (24).

Appendix D. Steady-state solution of equation (21)

We seek a quasi-static power law solution, $\omega_\tau(s) = H/s^\alpha$, to equation (27). Substituting to the left-hand side of

equation (27) one has

$$\int_s^\infty ds' \lambda(s|s') \omega_\tau(s') = -\frac{QH}{s^{\alpha+\nu-1}} \int_0^1 dy y^{\nu-2+\alpha} \int_y^{1-y} dx \zeta(x), \quad (\text{D.1})$$

after changing variables to $y = s/s'$. Here we took the well-defined limit $N \rightarrow \infty$ since the solution we seek should be independent of the tail's length. The only value of α for which equation (D.1) is zero is $\alpha = 2 - \nu$. The self-consistency of the quasi-static solution, equation (28), can be verified by substitution in equation (21) and showing that for loop sizes where the solution is valid ($s < s_\tau^{\max}$) corrections arising from integration over $s' > s_\tau^{\max}$ are small.

References

1. P.G. de Gennes, *Adv. Colloid Interface Sci.* **27**, 189 (1987).
2. G.J. Fleer, M.A. Cohen Stuart, J.M.H.M. Scheutjens, T. Cosgrove, B. Vincent, *Polymers at Interfaces* (Chapman and Hall, London, 1993).
3. E. Bouchaud, M. Daoud, *J. Phys. (Paris)* **48**, 1991 (1987).
4. P.G. de Gennes, *Some dynamical features of adsorbed polymers*, in *Molecular Conformation and Dynamics of Macromolecules in Condensed Systems*, edited by N. Nagasawa (Elsevier, Amsterdam, 1988) pp. 315-331.
5. P.G. de Gennes, *Dynamics of adsorbed polymers*, in *New Trends in Physics and Physical Chemistry of Polymers*, edited by Lieng-Huang Lee (Plenum Press, New York, 1989) pp. 9-18.
6. A.N. Semenov, J.-F. Joanny, *J. Phys. II* **5**, 859 (1995).
7. L.T. Lee, O. Guiselin, B. Farnoux, A. Lapp, *Macromolecules* **24**, 2518 (1991).
8. L. Auvray, J.P. Cotton, *Macromolecules* **20**, 202 (1987).
9. M. Kawaguchi, A. Takahashi, *Macromolecules* **16**, 1465 (1983).
10. P.G. de Gennes, *Macromolecules* **14**, 1637 (1981).
11. P.G. de Gennes, P. Pincus, *J. Phys. (Paris) Lett.* **44**, L241 (1983).
12. E. Eisenriegler, *J. Chem. Phys.* **79**, 1052 (1983).
13. P.G. de Gennes, *C. R. Acad. Sci. Paris Ser. II* **294**, 1317 (1982).
14. M. Aubouy, O. Guiselin, E. Raphael, *Macromolecules* **29**, 7261 (1996).
15. A.N. Semenov, J.-F. Joanny, *Europhys. Lett.* **29**, 279 (1995).
16. J.M.H.M. Scheutjens, G.J. Fleer, *J. Phys. Chem.* **83**, 1619 (1979).
17. J.M.H.M. Scheutjens, G.J. Fleer, *J. Phys. Chem.* **84**, 178 (1980).
18. I.S. Jones, P. Richmond, *J. C. S. Faraday Trans. II* **73**, 1062 (1977).
19. A.N. Semenov, J. Bonet-Avalos, A. Johner, J.F. Joanny, *Macromolecules* **29**, 2179 (1996).
20. A. Johner, J. Bonet-Avalos, C.C. van der Linden, A.N. Semenov, J.F. Joanny, *Macromolecules* **29**, 3629 (1996).
21. P.-Y. Lai, *J. Chem. Phys.* **103**, 5742 (1995).
22. R. Zajac, A. Chakrabarti, *J. Chem. Phys.* **104**, 2418 (1996).
23. J. de Joannis, C.-W. Park, J. Thomatos, I.A. Bitsanis, *Langmuir* **17**, 69 (2001).
24. E. Pefferkorn, A. Carroy, R. Varoqui, *J. Polym. Sci. Polym. Phys. Ed.* **23**, 1997 (1985).
25. E. Pefferkorn, A. Haouam, R. Varoqui, *Macromolecules* **22**, 2677 (1989).
26. R. Varoqui, E. Pefferkorn, *Progr. Colloid Polym. Sci.* **83**, 96 (1990).
27. P. Frantz, S. Granick, *Phys. Rev. Lett.* **66**, 899 (1991).
28. P. Frantz, S. Granick, *Macromolecules* **27**, 2553 (1994).
29. H.M. Schneider, S. Granick, *Macromolecules* **25**, 5054 (1992).
30. H.E. Johnson, S. Granick, *Macromolecules* **23**, 3367 (1990).
31. H.M. Schneider, P. Frantz, S. Granick, *Langmuir* **12**, 994 (1996).
32. J.F. Douglas, H.M. Schneider, P. Frantz, R. Lipman, S. Granick, *J. Phys. Condens. Matter* **9**, 7699 (1997).
33. P. Frantz, S. Granick, *Macromolecules* **28**, 6915 (1995).
34. I. Soga, S. Granick, *Macromolecules* **31**, 5450 (1998).
35. I. Soga, S. Granick, *Colloids Surf. A* **170**, 113 (2000).
36. Z. Fu, M. Santore, *Macromolecules* **31**, 7014 (1998).
37. Z. Fu, M. Santore, *Macromolecules* **32**, 1939 (1999).
38. E. Mubarekyan, M.M. Santore, *Macromolecules* **34**, 4978 (2001).
39. E. Mubarekyan, M.M. Santore, *Macromolecules* **34**, 7504 (2001).
40. U. Raviv, J. Klein, T.A. Witten, *Eur. Phys. J. E* **9**, 405; 425 (2002); A. Johner, A.N. Semenov, *Eur. Phys. J. E* **9**, 413 (2002); J.-U. Sommer, *Eur. Phys. J. E* **9**, 417 (2002); S. Granick, *Eur. Phys. J. E* **9**, 421 (2002).
41. P.O. Brown, D. Botstein, *Nat. Genet. Suppl.* **21**, 33 (1999).
42. V. Hlady, J. Buijs, *Curr. Opin. Biotechnol.* **7**, 72 (1996).
43. M.D. Joesten, L.J. Schaadt, *Hydrogen Bonding* (Marcel Dekker, New York, 1974).
44. T.J. Lenk, V.M. Hallmark, J.F. Rabolt, *Macromolecules* **26**, 1230 (1993).
45. J.B. Schlenoff, J.R. Dharia, H. Xu, L. Wen, M. Li, *Macromolecules* **28**, 4290 (1995).
46. J.S. Shaffer, A.K. Chakraborty, *Macromolecules* **26**, 1120 (1993).
47. P.M. Adriani, A.K. Chakraborty, *J. Chem. Phys.* **98**, 4263 (1993).
48. T. Cosgrove, C.A. Prestidge, A.M. King, B. Vincent, *Langmuir* **8**, 2206 (1992).
49. R. Laible, K. Hamann, *Adv. Colloid Interface Sci.* **13**, 65 (1980).
50. C. Creton, E.J. Kramer, H.R. Brown, C.-Y. Hui, *Adv. Polym. Sci.* **156**, 53 (2001).
51. U. Sundararaj, C. Macosko, *Macromolecules* **28**, 2647 (1995).
52. B. O'Shaughnessy, D. Vavylonis, *Macromolecules* **32**, 1785 (1999).
53. I. Lee, R.P. Wool, *Macromolecules* **33**, 2680 (2000).
54. S. Wu, *Polymer Interface Adhesion* (Marcel Dekker, New York, 1982).
55. D.C. Edwards, J. Mater. Sci. **25**, 4175 (1990).
56. J.P. Cohen Addad, *Polymer* **30**, 1820 (1989).
57. J.P. Cohen Addad, L. Dujourdy, *Polym. Bull.* **41**, 253 (1998).
58. L. Auvray, P. Auroy, M. Cruz, *J. Phys. I* **2**, 943 (1992).
59. L. Auvray, M. Cruz, P. Auroy, *J. Phys. II* **2**, 1133 (1992).

60. C.J. Durning, B. O'Shaughnessy, U. Sawhney, D. Nguyen, J. Majewski, G.S. Smith, *Macromolecules* **32**, 6772 (1999).
61. C. Marzolin, P. Auroy, M. Deruelle, J.P. Folkers, L. Léger, A. Menelle, *Macromolecules* **34**, 8694 (2001).
62. L. Léger, E. Raphaël, H. Hervet, *Adv. Polym. Sci.* **138**, 185 (1999).
63. M. Deruelle, M. Tirrell, Y. Marciano, H. Hervet, L. Léger, *Faraday Discuss.* **98**, 55 (1994).
64. O. Guiselin, *Europhys. Lett.* **17**, 225 (1992).
65. J.P. Cohen Addad, P.G. de Gennes, *C. R. Acad. Sci. Paris Ser. II* **319**, 25 (1994).
66. B. O'Shaughnessy, D. Vavylonis, submitted to *Europhys. Lett.*, cond-mat/0303094.
67. W. Barford, R.C. Ball, C.M.M. Nex, *J. Chem. Soc., Faraday Trans. 1* **82**, 3233 (1986).
68. W. Barford, R.C. Ball, *J. Chem. Soc., Faraday Trans. 1* **83**, 2515 (1987).
69. K. Konstadinidis, S. Prager, M. Tirrell, *J. Chem. Phys.* **97**, 7777 (1992).
70. J.S. Shaffer, *Macromolecules* **27**, 2987 (1994).
71. A.L. Ponomarev, T.D. Sewell, C.J. Durning, *Macromolecules* **33**, 2662 (2000).
72. J. Talbot, G. Tarjus, P.R. Van Tassel, P. Viot, *Colloids Surf.* **165**, 287 (2000).
73. K. Konstadinidis, B. Thakkar, A. Chakraborty, L.W. Potts, R. Tannenbaum, M. Tirrell, J.F. Evans, *Langmuir* **8**, 1307 (1992).
74. B. O'Shaughnessy, D. Vavylonis, *Europhys. Lett.* **45**, 638 (1999).
75. B. O'Shaughnessy, *Bulk and interfacial polymer reaction kinetics*, in *Theoretical and Mathematical Models in Polymer Science*, edited by A. Grosberg (Academic Press, New York, 1998) Chapt. 5, pp. 219–275.
76. B. O'Shaughnessy, D. Vavylonis, *Phys. Rev. Lett.* **90**, 056103 (2003).
77. B. Duplantier, *J. Stat. Phys.* **54**, 581 (1989).
78. K. De'Bell, T. Lookman, *Rev. Mod. Phys.* **65**, 87 (1993).
79. P.G. de Gennes, *Scaling Concepts in Polymer Physics* (Cornell University Press, Ithaca, New York, 1985).
80. Equation (19) describes a fragmentation process and appears in many branches of physics, e.g., the Altarelli-Parisi equation in QCD. (Z. Cheng, S. Redner, *J. Phys. A* **23**, 1233 (1990); S. Redner, in *Statistical Methods for the Fracture of Disordered Media*, edited by H.J. Herman, S. Roux (Elsevier Science Publishers B. V., Amsterdam, 1990) pp. 321–348; E.D. McGrady, R.M. Ziff, *Phys. Rev. Lett.* **58**, 892 (1987)).
81. M. Doi, S.F. Edwards, *The Theory of Polymer Dynamics* (Clarendon Press, Oxford, 1986).
82. J.S. Shaffer, A.K. Chakraborty, M. Tirrell, H.T. Davis, J.L. Martins, *J. Chem. Phys.* **95**, 8616 (1991).
83. A.K. Chakraborty, J.S. Shaffer, P.M. Adrani, *Macromolecules* **24**, 5226 (1991).
84. M.-W. Tsao, K.-H. Pfeifer, J.F. Rabolt, D.G. Castner, L. Haussling, H. Ringsdorf, *Macromolecules* **30**, 5913 (1997).
85. T. Cosgrove, C.A. Prestidge, B. Vincent, *J. Chem. Soc. Faraday Trans.* **86**, 1377 (1990).
86. T. Cosgrove, A. Patel, J.R.P. Webster, A. Zarbakhsh, *Langmuir* **9**, 2326 (1993).
87. B. O'Shaughnessy, D. Vavylonis, *Phys. Rev. Lett.* **84**, 3193 (2000).
88. B. O'Shaughnessy, D. Vavylonis, *Eur. Phys. J. E* **1**, 159 (2000).
89. P.G. de Gennes, *J. Chem. Phys.* **76**, 3316 (1982).
90. D.J. Amit, G. Parisi, L. Peliti, *Phys. Rev. B* **27**, 1635 (1983).
91. L. Pietronero, *Phys. Rev. Lett.* **55**, 2025 (1985).
92. W. Feller, *An Introduction to Probability Theory and Its Applications*, Vol. **2**, 2nd ed. (John Wiley & Sons, Inc., New York, 1971).